

# Global Biogeochemical Cycles<sup>®</sup>



# **RESEARCH ARTICLE**

10.1029/2022GB007403

#### **Key Points:**

- Permafrost landscape history regulates fluvial carbon (C) sources and export across a transect of continental glaciation and thermokarst
- Fluvial C flux equaled 6%–16% of vegetation C uptake in most watersheds and 60% in those affected by permafrost thaw-driven mass wasting
- Thaw-susceptible terrains will be significant to Arctic ecosystem carbon balance as permafrost thaw and hydrologic carbon fluxes intensify

#### **Supporting Information:**

Supporting Information may be found in the online version of this article.

#### Correspondence to:

S. Zolkos, sgzolkos@gmail.com

#### Citation:

Zolkos, S., Tank, S. E., Kokelj, S. V., Striegl, R. G., Shakil, S., Voigt, C., et al. (2022). Permafrost landscape history shapes fluvial chemistry, ecosystem carbon balance, and potential trajectories of future change. *Global Biogeochemical Cycles*, *36*, e2022GB007403. https://doi.org/10.1029/2022GB007403

Received 28 MAR 2022 Accepted 16 AUG 2022

© 2022. The Authors.
This is an open access article under the terms of the Creative Commons Attribution License, which permits use, distribution and reproduction in any medium, provided the original work is properly cited.

# Permafrost Landscape History Shapes Fluvial Chemistry, Ecosystem Carbon Balance, and Potential Trajectories of Future Change

Scott Zolkos<sup>1,2,3</sup> D, Suzanne E. Tank<sup>1</sup> D, Steven V. Kokelj<sup>4</sup>, Robert G. Striegl<sup>5</sup> D, Sarah Shakil<sup>1</sup> D, Carolina Voigt<sup>6,7</sup>, Oliver Sonnentag<sup>6</sup>, William L. Quinton<sup>8</sup> D, Edward A. G. Schuur<sup>9</sup> D, Donatella Zona<sup>10,11</sup>, Peter M. Lafleur<sup>12</sup>, Ryan C. Sullivan<sup>13</sup> D, Masahito Ueyama<sup>14</sup> D, David Billesbach<sup>15</sup> D, David Cook<sup>13</sup>, Elyn R. Humphreys<sup>16</sup> D, and Philip Marsh<sup>8</sup> D

<sup>1</sup>Department of Biological Sciences, University of Alberta, Edmonton, AB, Canada, <sup>2</sup>Now at John A. Paulson School of Engineering and Applied Sciences, Harvard University, Cambridge, MA, USA, <sup>3</sup>Now at Woodwell Climate Research Center, Falmouth, MA, USA, <sup>4</sup>Northwest Territories Geological Survey, Yellowknife, NT, Canada, <sup>5</sup>United States Geological Survey, Boulder, CO, USA, <sup>6</sup>Département de géographie and Centre d'Études Nordiques, Université de Montréal, Montreal, QC, Canada, <sup>7</sup>Department of Environmental and Biological Sciences, University of Eastern Finland, Kuopio, Finland, <sup>8</sup>Cold Regions Research Centre, Wilfrid Laurier University, Waterloo, ON, Canada, <sup>9</sup>Center for Ecosystem Science and Society and Department of Biological Sciences, Northern Arizona University, Flagstaff, AZ, USA, <sup>10</sup>Department of Biology, San Diego State University, San Diego, CA, USA, <sup>11</sup>Department of Animal and Plant Sciences, University of Sheffield, UK, <sup>12</sup>School of the Environment, Trent University, Peterborough, ON, Canada, <sup>13</sup>Environmental Science Division, Argonne National Laboratory, Lemont, IL, USA, <sup>14</sup>Graduate School of Life and Environmental Sciences, Osaka Prefecture University, Sakai, Japan, <sup>15</sup>Department of Biological Systems Engineering, University of Nebraska–Lincoln, Lincoln, NE, USA, <sup>16</sup>Geography and Environmental Studies, Carleton University, Ottawa, ON, Canada

**Abstract** Intensifying permafrost thaw alters carbon cycling by mobilizing large amounts of terrestrial substrate into aquatic ecosystems. Yet, few studies have measured aquatic carbon fluxes and constrained drivers of ecosystem carbon balance across heterogeneous Arctic landscapes. Here, we characterized hydrochemical and landscape controls on fluvial carbon cycling, quantified fluvial carbon fluxes, and estimated fluvial contributions to ecosystem carbon balance across 33 watersheds in four ecoregions in the continuous permafrost zone of the western Canadian Arctic: unglaciated uplands, ice-rich moraine, and organic-rich lowlands and till plains. Major ions, stable isotopes, and carbon speciation and fluxes revealed patterns in carbon cycling across ecoregions defined by terrain relief and accumulation of organics. In previously unglaciated mountainous watersheds, bicarbonate dominated carbon export (70% of total) due to chemical weathering of bedrock. In lowland watersheds, where soil organic carbon stores were largest, lateral transport of dissolved organic carbon (50%) and efflux of biotic CO<sub>2</sub> (25%) dominated. In watersheds affected by thaw-induced mass wasting, erosion of ice-rich tills enhanced chemical weathering and increased particulate carbon fluxes by two orders of magnitude. From an ecosystem carbon balance perspective, fluvial carbon export in watersheds not affected by thaw-induced wasting was, on average, equivalent to 6%-16% of estimated net ecosystem exchange (NEE). In watersheds affected by thaw-induced wasting, fluvial carbon export approached 60% of NEE. Because future intensification of thermokarst activity will amplify fluvial carbon export, determining the fate of carbon across diverse northern landscapes is a priority for constraining trajectories of permafrost region ecosystem carbon balance.

Plain Language Summary Freshwaters are a main component of the global carbon cycle and climate. Yet, their role in climate change is uncertain in permafrost regions, where thaw is releasing large amounts of carbon and enabling production of climate-warming greenhouse gases. To reduce uncertainty, we measured stream chemistry and carbon fluxes across four ecoregions including a global hotspot of permafrost thaw in the western Canadian Arctic. Comparing across ecoregions, lowlands were strong sources of biological carbon dioxide and methane to the atmosphere; mountain rivers ferried products from chemical rock weathering downstream; and streams affected by permafrost thaw-induced wasting transported large amounts of particulate carbon. Typical of northern ecosystems, carbon fluxes in non-thaw-affected streams were equivalent to 6%–16% of carbon uptake by terrestrial vegetation. However, in watersheds affected by thaw-induced wasting, carbon fluxes were up to 100 times higher and approached 60% of vegetation carbon uptake. Together, these findings

ZOLKOS ET AL. 1 of 21

reveal that thermokarst-susceptible terrains are poised to emerge as a significant component of the Arctic ecosystem carbon balance and global climate feedbacks, due to hydrologic carbon fluxes that will intensify as permafrost thaw accelerates.

#### 1. Introduction

At northern high latitudes, permafrost thaw and intensifying hydrologic cycles are strengthening terrestrial-freshwater linkages (Vonk et al., 2019) and the aquatic component of ecosystem carbon cycling and climate feedbacks (Plaza et al., 2019; Turetsky et al., 2020). The intensification of these processes across northern watersheds is reflected by multi-decadal increases in riverine solute fluxes and the propagation of thawed permafrost substrate across watershed scales (Drake, Tank, et al., 2018; Kokelj et al., 2021; Toohey et al., 2016; Zolkos et al., 2018). Reactivation of thawed permafrost substrate into modern biogeochemical cycles manifests as perturbation to local and regional carbon cycling. For instance, on the Peel Plateau in the Northwest Territories of Canada, thaw-driven mass wasting of ice- and mineral-rich glacigenic deposits in fluvial network headwaters (Kokelj et al., 2013) increases particulate organic carbon (POC) export by orders of magnitude (Shakil et al., 2020) and enables production of dissolved inorganic carbon (DIC =  $\Sigma[CO_7, HCO_3^-, CO_3^{2-}]$ ) via chemical weathering of carbonate-bearing tills (Zolkos & Tank, 2020). In comparison, thaw of relatively biolabile permafrost organic carbon in previously unglaciated terrains (Strauss et al., 2017) can fuel relatively high rates of microbial oxidation of dissolved organic carbon (DOC) and increase carbon dioxide (CO<sub>2</sub>) loss within fluvial network headwaters (Drake, Guillemette, et al., 2018). Variation in landscape conditions (e.g., topography, hydrology, and geology) across the northern permafrost zone are hypothesized to underlie thaw effects on aquatic carbon cycling (Tank et al., 2020), yet few studies have assessed physiographic controls on aquatic carbon cycling within thaw-susceptible terrains.

At the landscape scale, vertical exchange of fluvial CO<sub>2</sub> and methane (CH<sub>4</sub>) with the atmosphere (henceforth, "efflux") and lateral downstream fluxes of DIC, DOC, and particulate carbon (PC) represent carbon losses from watersheds that are counterbalanced by vegetation photosynthesis. The degree to which ecosystem carbon uptake via photosynthesis offsets aquatic and terrestrial carbon losses determines the net ecosystem carbon balance (NECB), which broadly describes whether landscapes are carbon sources or sinks (Chapin et al., 2006). From a watershed perspective, the ecosystem carbon balance is comprised of net terrestrial carbon uptake as CO<sub>2</sub> (i.e., net ecosystem exchange [NEE], the difference between two large component fluxes, gross primary productivity [GPP] and ecosystem respiration), and vertical exchange of carbon gases (CO<sub>2</sub>, CH<sub>4</sub>, CO, and volatile organic carbon) between the land and atmosphere, and lateral aquatic export of dissolved and PC (Chapin et al., 2006). Previous comparisons of aquatic carbon fluxes and NEE in western Siberia (Karlsson et al., 2021), Scandinavia (Lundin et al., 2016; Wallin et al., 2013), sub-arctic Canada (Hutchins et al., 2020), Alaska (McGuire et al., 2018), and the Qinghai-Tibet Plateau (Song et al., 2020) indicate that aquatic carbon fluxes in northern environments are generally equivalent to 10%-20% of NEE, but vary regionally. In remote northern regions, where field-based measurements of NEE can be sparse (Pallandt et al., 2022), estimates of ecosystem carbon balance are supported by measurements of aquatic carbon fluxes combined with modeled estimates of NEE informed by remotely sensed ecosystem properties (Kimball et al., 2018). Using this approach in the Ob' river basin in western Siberia, where low terrain relief and carbon accumulation over millennia have promoted development of vast peat wetlands, Karlsson et al. (2021) found that aquatic carbon efflux was almost 10 times larger than lateral export to the Arctic Ocean and was equivalent to 35%-50% of the net terrestrial carbon uptake. Across Sweden and Alaska, aquatic carbon efflux is similar in magnitude to lateral carbon fluxes (Humborg et al., 2010; Stackpoole et al., 2017). Observations on the species comprising aquatic carbon fluxes, physiographic controls on aquatic carbon fluxes, and estimates of aquatic contributions to NECB remain sparse for arctic Canada, where continental glaciation shaped the evolution of high-latitude ecosystems.

In this study, we measure fluvial chemistry across diverse permafrost terrains to understand how geology and landscape evolution since the last glacial maximum (LGM) have shaped modern-day variation in carbon sources, fluxes, and ecosystem carbon balance. We focus on the western Canadian Arctic, where variation in geology, topography, hydrology, and glacial history have driven four adjacent ecoregions to evolve along different trajectories (Figure 1). These four ecoregions cover nearly 84,000 km<sup>2</sup> of the northern Yukon Territory and western Northwest Territories (Ecosystem Classification Group, 2009, 2010; Kokelj, Tunnicliffe, et al., 2017; Smith et al., 2004) and include: (a) the previously unglaciated Richardson Mountains; (b) the ice-rich and thermokarst-susceptible

ZOLKOS ET AL. 2 of 21

elibrary.wiley.com/doi/10.1029/2022GB007403 by University Of Alaska Fairbanks, Wiley Online Library on [17/02/2023]. See the Terms and Conditions (https://onlinelibrary.wile

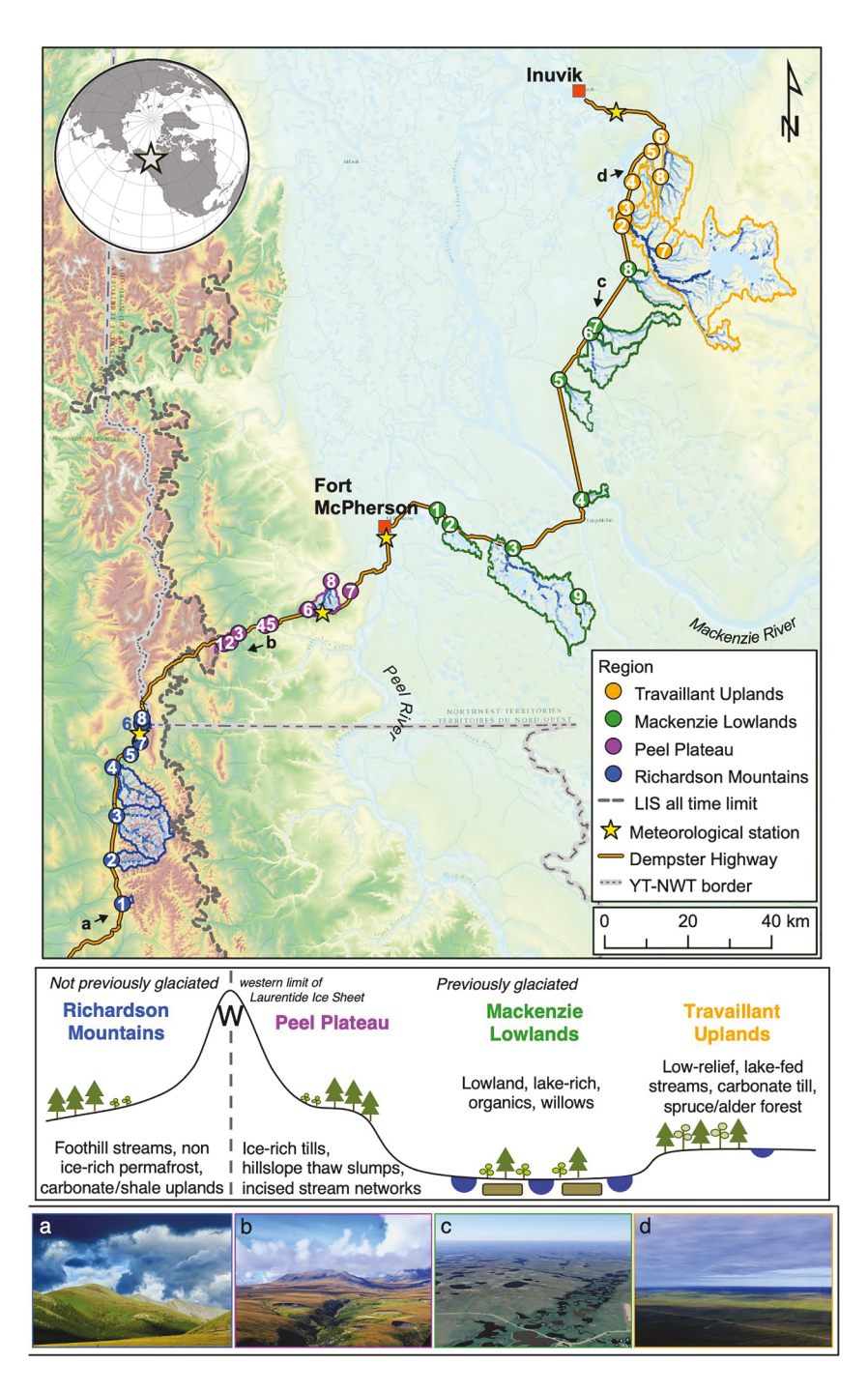


Figure 1. Map of sampling sites within each region (upper panel) aligned with cross-section of terrain characteristics of the four study regions (middle panel) depicted in photos (lower panel): (a) Richardson Mountains, (b) Peel Plateau, (c) Mackenzie Lowlands, and (d) Travaillant Uplands. In upper panel, site numbers are shown within or adjacent to symbols, and letters and arrows correspond to approximate locations and directions of photos in lower panel. Image of Mackenzie Lowlands from Google Earth. Laurentide Ice Sheet western limit from the literature (Duk-Rodkin & Hughes, 1992a, 1992b). Base map from ESRI ArcGIS Online.

glacial tills of the Peel Plateau; (c) the organic-rich till plains of the Mackenzie Lowlands; and (d) the rolling till plains of the Travaillant Uplands. This transect of glacial history and topography-driven variation in hydrology and organic carbon accumulation (Table 1) provides an ideal setting to determine how variation in permafrost landscape type gives rise to regional patterns in modern-day fluvial chemistry, carbon cycling, and ecosystem

ZOLKOS ET AL. 3 of 21

**Table 1** *Physiographic Conditions of the Study Regions* 

Parameter	Units	Richardson Mountains	Peel Plateau	Mackenzie Lowlands	Travaillant Uplands
Ecoregion characteristics	and meteorolo	gical conditions			
Ecoregion correlation	-	British-Richardson Mountains	Tundra Cordillera high subarctic ecoregion	Arctic Red Plain high subarctic ecoregion	Travaillant Upland high subarctic ecoregion
Ecoregion area	$km^2$	26,690	7,828	22,907	26,389
Elevation	masl	450–900	100–750	25–350	50-450
MSAT	°C	11.8	12.8	14.5	13.2
TSP	mm	74	238	-	112
Watershed characteristics					
Slope	0	14.8 (2.1)	5.7 (1.4)	0.8 (0.1)	1.2 (0.2)
Elevation	m	815 (35)	503 (68)	88 (12)	156 (14)
Area	$km^2$	28 (16)	6 (5)	62 (24)	102 (74)
Carbonate	%	60 (18)	0	0	0
Silicate	%	40 (18)	100 (0)	100(0)	100 (0)
Colluvial	%	93 (3)	40 (18)	0.4 (0.4)	0.2 (0.2)
Fluvial	%	6 (3)	0	0	0
Moraine	%	0	60 (18)	60 (9)	92 (4)
Organic	%	1(1)	0	39 (9)	7 (4)
Lakes/ponds	%	0	0.2 (0.1)	18 (7)	7 (2)
SOC	$kgC m^{-2}$	16.3 (3.9)	21.4 (0.2)	70.5 (2.1)	29.8 (5.2)
GPP	$gC m^{-2} d^{-1}$	3.3 (0.2)	5.5 (0.2)	5.7 (0.3)	5.8 (0.2)
NEE	gC m <sup>-2</sup> d <sup>-1</sup>	-0.65 (0.02)	-0.70 (0.03)	-0.82 (0.02)	-0.60 (0.09)

Note. Ecoregion correlations and areas from the literature (Ecosystem Classification Group, 2009, 2010; Smith et al., 2004). MSAT = mean summer (June–August) air temperature. TSP = total summer precipitation. Elevation, Slope, and Area = mean watershed elevation, slope, and area. Carbonate and Silicate = distribution of carbonate and silicate bedrock, respectively (sum =  $\sim$ 100) (Norris, 1985). Colluvial, Fluvial, Moraine, Organic = distribution of surficial geology deposits (sum =  $\sim$ 100) (Côté et al., 2013; Lipovsky & Bond, 2014). Distribution of lakes and ponds from Natural Resources Canada (https://open.canada.ca). SOC = soil organic carbon content from 0 to 100 cm (Hugelius et al., 2013). GPP = gross primary productivity (Running et al., 2015). NEE = net ecosystem exchange (Kimball et al., 2018).

carbon balance, and dictates potential trajectories of future change. We tested three hypotheses. First, that stream water chemistry and carbon species would show systematic variation reflective of the divergent physiographic conditions among the four ecoregions. Second, that total fluvial carbon yields (i.e., flux divided by watershed area) would be highest in unglaciated uplands, where greater terrain relief, streamflow, and exposed bedrock enhances weathering and lateral inorganic carbon fluxes. Third, that lateral fluxes would be larger relative to NEE on the ice-rich till Peel Plateau, in particular where recent acceleration in hillslope thermokarst activity is known to mobilize carbon into fluvial networks. We sampled the outlets of 33 watersheds (0.1–610 km²) across these four regions (Figure 1) from June through August 2016 and combined measurements of stream chemistry, CO<sub>2</sub> and CH<sub>4</sub> efflux, and hydrology with geospatial landscape characteristics and modeled estimates of growing season NEE derived from remotely sensed data. Our findings reveal how physiography shapes variation in biogeochemical cycling and fluvial contributions to ecosystem carbon balance.

#### 2. Methods

#### 2.1. Study Regions

Across the circumpolar North, a range of physiographic conditions (e.g., geology, glacial history, and hydrology) together with Holocene climate change have given rise to regional variation in ecosystems, the composition of soils and permafrost, and hydrology. This is exemplified in the western Canadian Arctic, where we focus on four adjacent ecoregions that span a transect of continental glaciation (Figure 1). In contrast to ecosystems west of the Richardson Mountains, the three previously glaciated terrains located to the east, within the Mackenzie

ZOLKOS ET AL. 4 of 21

River delta region, represent variation in topography, permafrost ground ice and soil conditions, and mass wasting intensity. This gives rise to large regional differences in the distribution of organic soils and thaw-driven mobilization of permafrost substrate into contemporary biogeochemical cycles (Hugelius et al., 2014; Kokelj, Tunnicliffe, et al., 2017).

The previously unglaciated Richardson Mountains (ecoregion 1) demarcates the western limit of the former Laurentide Ice Sheet (LIS) during the LGM (Clark et al., 2009; Ehlers et al., 2011) and was shaped by mass wasting, colluviation, and weathering of shale, carbonate, and sandstone bedrock outcrops through the Pleistocene (Norris, 1985; Smith et al., 2004). Mountain peaks reach 1,600 masl and upper slopes are veneered by mostly unvegetated colluvium, which transitions into tussock- and shrub-tundra on pediment surfaces at lower elevations, with stands of white spruce in sheltered valleys of larger rivers. Thaw-driven landslides are not common in the Richardson Mountains, where watersheds are dominated by exposed bedrock and colluvium. Regional observations of icings indicate potential contributions from groundwater to fluvial networks in mountainous terrains west of the LIS limit (Crites et al., 2020). A structural and topographic depression separates uplifted shales in the northern Richardson Mountain watersheds (sites RM-6 to RM-8) from folded and exposed limestone and sandstone in the southern watersheds (RM-1 to RM-5) (Norris, 1985; Smith et al., 2004) (Figure 1).

Western headwaters of the Peel Plateau (ecoregion 2) region are sparsely vegetated mountain slopes which consist mainly of colluvium from exposed marine shale and sandstone bedrock (Duk-Rodkin & Hughes, 1992b; Norris, 1985) and transition into tussock- and shrub-tundra on the plateau and open spruce forest at lower elevations (Kokeli, Tunnicliffe, et al., 2017). The plateau is a fluvially incised hillslope plateau within a glacial margin depositional environment hosting ice-rich landslide-susceptible tills that are mantled by deposits hosting modern organic carbon (Kokelj, Tunnicliffe, et al., 2017). Expansion of the LIS eroded regional Mesozoic and Paleozoic shales, sandstones, and limestones, and its retreat ~18 kybp (Lacelle et al., 2013) emplaced carbonate, sulfide, and silicate bearing tills on the Peel Plateau (Zolkos & Tank, 2020) via burial and preservation of basal glacier ice and development of segregated ground ice (Kokelj, Tunnicliffe, et al., 2017). The modern-day Peel Plateau contains ice-rich hummocky moraine, glaciofluvial, glaciolacustrine, and colluvial deposits with permafrost up to 50 m in thickness (Kokelj, Tunnicliffe, et al., 2017). Rapid warming and intensifying precipitation are accelerating thaw-induced mass wasting in the form of retrogressive thaw slump (RTS) thermokarst features along the Peel Plateau and in glacial margins elsewhere across northwestern Canada (Kokelj, Lantz, et al., 2017; Segal et al., 2016). Valleys in fluvial network headwaters promote development of RTS hillslope thermokarst features (Segal et al., 2016) and associated downslope wasting of tens to millions of cubic meters of thawed sediments (van der Sluijs et al., 2018). These sediments now exceed the transport capacity of streams by orders of magnitude and are altering geochemical fluxes and ecosystem function across watershed scales (Kokelj et al., 2021). RTS activity covers only a small areal proportion of watersheds, yet propagates a sediment- and solute-rich slurry containing thawed permafrost substrate that is dominated by particulates and cascades across watershed scales via fluvial processes (Bröder et al., 2021; Kokelj et al., 2013; Malone et al., 2013; Shakil et al., 2020; Zolkos et al., 2020).

In the Mackenzie Lowlands (ecoregion 3) and Travaillant Uplands (ecoregion 4), and in permafrost peatlands elsewhere across western Canada, relatively large stores of organic carbon are increasingly susceptible to thaw (Hugelius et al., 2020). The geology of the Mackenzie Lowlands and Travaillant Uplands is similar: both regions contain LIS-derived tills of variable thicknesses atop Devonian and Cretaceous age sandstone and shale bedrock (Norris, 1985). Organic carbon-rich Holocene permafrost peatlands are widespread in the low-relief, poorly drained Mackenzie Lowlands (Burn & Kokelj, 2009), where streams connect thousands of small thermokarst lakes and ponds (Duk-Rodkin & Hughes, 1992a, 1992b) among black spruce-dominated forest, and willow fens (Ecosystem Classification Group, 2009). In the Travaillant Uplands, lake-fed streams have developed across an elevational gradient and flow through relatively organic-rich peatlands (Duk-Rodkin & Hughes, 1992a) and across hummocky plains and open spruce forest (Ecosystem Classification Group, 2009; Norris, 1985).

#### 2.2. Stream Sampling

We sampled streams at 33 sites along a 300 km transect accessed by the Dempster Highway from near Rock River, Yukon Territory, to near Inuvik in the Northwest Territories (Figure 1). Streams in most regions spanned Strahler orders 1–5 and were chosen to reflect the varied environmental conditions within and among regions. Sites were visited three times each from June to August 2016 (Table S1 in Supporting Information S1). During each site

ZOLKOS ET AL. 5 of 21

visit, water temperature, specific conductance, dissolved oxygen, and pH were measured using a pre-calibrated YSI Professional-Plus water quality meter, and samples were collected to determine concentrations of DIC, DOC,  $CO_2$ , and  $CH_4$ . Samples for dissolved  $CO_2$  and  $CH_4$  concentrations were collected following the headspace equilibration method (Hesslein et al., 1991). We also sampled for cations  $(Ca^{2+}, Mg^{2+}, Na^+, and K^+)$  and anions  $(SO_4^{2-}, Mg^{2+})$  and  $(Ca^{2+}, Mg^{2+})$  to constrain sources of mineral weathering; chromophoric dissolved organic matter, to characterize organic matter (specific UV absorbance at 254 nm  $[SUVA_{254}]$  and spectral slope ratio  $[S_R]$ ); and for dissolved iron (dFe), to correct  $(Ca^{2+}, Mg^{2+})$  measurements. To further constrain the carbon balance, we collected total suspended solids in a subset of streams to determine total PC concentrations. This subset was also sampled for total dissolved nitrogen (TDN) and dissolved inorganic nitrogen (DIN =  $(Ca^{2+}, Mg^{2+}, NO_3^+, NO_2^-)$ ) to characterize inorganic nutrient status among regions, and stable isotopes of DIC  $(Ca^{2+}, NG^+, NO_3^+, NO_2^-)$ ) to constrain dissolved carbon sources. At each site at the end of the summer, we sampled streams for stable water isotopes  $(Ca^{2+}, NG^+, NG^+,$ 

The efflux (J) of CO<sub>2</sub> (µmol m<sup>-2</sup> s<sup>-1</sup>) was measured in triplicate using an EGM-4 (PP Systems) connected to a stationary streamlined transparent chamber (Crawford et al., 2013). Discrete CH<sub>4</sub> samples were collected every 5 min for a single 20-min period from a port in the Bev-a-line tubing, stored, and later analyzed in the same fashion as dissolved  $CH_4$  samples to determine  $J_{CH4}$  (nmol m<sup>-2</sup> s<sup>-1</sup>) (Methods S2 in Supporting Information S1). Measurements were made at each site at the beginning and end of the summer, and  $J_{\rm CO2}$  and  $J_{\rm CH4}$  were calculated as  $J = PH\Delta C/RT\Delta t \times c$  (Duc et al., 2013), where P is atmospheric pressure (atm); H is flux chamber height (m);  $\Delta C$  is the change in headspace gas (ppmv); R is the ideal gas constant (82.0562 mL atm K<sup>-1</sup> mol<sup>-1</sup>); T is air temperature (°K);  $\Delta t$  is measurement duration (s); and c converts from mol to  $\mu$ mol (CO<sub>2</sub>) or nmol (CH<sub>4</sub>). CO<sub>2</sub> and CH<sub>4</sub> efflux data were quality-checked and 11 measurements of CH<sub>4</sub> efflux were omitted, owing to poor linearity due to variability in the data (n = 6) and  $CH_4$  loss from the chamber (n = 5) (Table S2 in Supporting Information S1). Gas transfer velocities  $(k, m d^{-1})$  of  $CO_2$  and  $CH_4$  were calculated for comparison to other studies, using J and the concentrations of dissolved gas (mol m<sup>-3</sup>) in the stream ( $c_{\text{water}}$ ) and in equilibrium with the atmosphere ( $c_{\text{sat}}$ ) (Cole & Caraco, 2001). Excess carbon gas, calculated as a proportion ( $c_{\text{water}}$ :  $c_{\text{sat}}$ ), was used to evaluate whether stream gas concentrations were oversaturated ( $c_{\rm excess} > 1$ , indicating gas loss to the atmosphere), undersaturated ( $c_{\text{excess}} < 1$ ), or in equilibrium ( $c_{\text{excess}} = 1$ ) with the atmosphere (Striegl et al., 2012). Additional details on gas efflux measurements are provided in Supporting Information S1.

#### 2.3. Fluvial Carbon Fluxes and Yields

Lateral constituent fluxes were calculated as the product of constituent concentration and instantaneous stream discharge. To estimate  $\mathrm{CO}_2$  and  $\mathrm{CH}_4$  efflux at the watershed scale, we summed the product of  $J_{\mathrm{CO}2}$  or  $J_{\mathrm{CH}4}$  and fluvial surface area for each stream order in each watershed (Campeau et al., 2014; Zolkos et al., 2019). Fluvial surface area in each watershed, estimated as the product of mean stream width from field measurements and total stream length for each stream order (Methods S3 in Supporting Information S1). To constrain the effects of varying  $J_{\mathrm{CO}2}$ ,  $J_{\mathrm{CH}4}$ , and stream width on upscaled efflux, we report the mean and range of upscaled fluvial  $J_{\mathrm{CO}2}$  and  $J_{\mathrm{CH}4}$ . These estimates do not capture fine-scale heterogeneity in aquatic gas efflux within individual stream reaches (e.g., Crawford et al., 2017), yet our sampling across stream orders attempts to capture variability in gas concentrations across scales (e.g., Hutchins et al., 2021) and allows for a first estimate of watershed-scale  $\mathrm{CO}_2$  and  $\mathrm{CH}_4$  efflux in western Arctic Canada. To assess how the types of carbon comprising fluvial fluxes varied among sites and regions, we calculated fluxes of individual carbon species relative to the total carbon flux at each site, henceforth termed proportional flux:  $p = \mathrm{species}$  flux/total flux, where total flux equals the sum of efflux ( $J_{\mathrm{CO}2}$  and  $J_{\mathrm{CH}4}$ ) and lateral fluxes of DIC, DOC, PIC, and POC.

To control for potential effects of watershed area on discharge and constituent concentration, constituent fluxes and stream discharge were normalized to watershed area to estimate daily constituent yields (µmol m<sup>-2</sup> d<sup>-1</sup>) and water yield (runoff; mm d<sup>-1</sup>). The relationship between carbon yield and runoff is useful for comparing watershed carbon sources and export, and reflects the degree to which carbon export may be limited by availabilities of carbon versus water (e.g., Striegl et al., 2005). The fluvial fluxes and yields that we estimate represent carbon export during the summer growing season. Varied environmental conditions during the year would likely

ZOLKOS ET AL. 6 of 21

impart seasonal variability if we had extended our observations beyond the summertime. We focus on spatial instead of temporal variability in our data due to low sampling frequency ( $n \le 3$  per site) (Table S1 in Supporting Information S1).

#### 2.4. Net Ecosystem Exchange and Fluvial Contributions to Ecosystem Carbon Balance

To assess the relative magnitudes of summertime fluvial and terrestrial carbon fluxes among the study regions, we compared our estimates of total fluvial carbon flux for each watershed with collocated estimates of mean NEE from June through August 2016. For this, we used the NASA Soil Moisture Active Passive Level 4 product (SPL4CMDL) (Kimball et al., 2018), which provides global gridded (9 km) daily estimates of NEE (CO<sub>2</sub>) using a satellite data-based terrestrial carbon flux model informed by satellite measurements of ecosystem properties including soil moisture, land cover, and vegetation, and the NASA Goddard Earth Observing System Model, version five (GEOS-5) land model assimilation system. For comparison with fluvial carbon fluxes in our study regions, we converted NEE estimates for each watershed to kgC d<sup>-1</sup>, first subtracting the surface area covered by freshwaters (streams, lakes/ponds) from the total watershed area to obtain terrestrial area. To determine relative contributions of fluvial and terrestrial carbon fluxes to ecosystem carbon balance, we normalized our daily estimates of lateral fluxes ( $\Sigma[DIC, DOC, PIC, and POC]$ ) and total efflux ( $\Sigma[J_{CO2}, J_{CH4}]$ ) to NEE. Additional information is available in Supporting Information S1.

#### 2.5. Geospatial Analyses

We used ArcHydro tools in ArcGIS 10.5 software to delineate watersheds from the Canadian Digital Elevation Model, which we reconditioned using satellite imagery-adjusted stream vectors from the Natural Resources Canada National Hydro Network (NHN; https://open.canada.ca). To constrain the varied potential landscape controls on carbon cycling and balance, we used published geospatial data to characterize the distributions of surficial and bedrock geology (Côté et al., 2013; Lipovsky & Bond, 2014; Norris, 1985), lakes and ponds (NHN), soil organic carbon content (SOC) in the upper 1 m of soil (Hugelius et al., 2013), and vegetation GPP (Running et al., 2015). Mean summer air temperature (°C) and total summer precipitation (mm) of the study regions were calculated from daily data collected by Environment and Climate Change Canada meteorological stations in Inuvik, Fort McPherson, and Rock River (http://climate.weather.gc.ca/), and a Government of Northwest Territories meteorological station located on the Peel Plateau. Full methods for deriving watershed topography, geology, and estimates of vegetation productivity can be found in Supporting Information S1.

#### 2.6. Statistics

Statistics were performed using R software v.3.4.4 (R Core Team, 2018). To test for variation in hydrochemical and environmental variables during the summer sampling period (Table S1 in Supporting Information S1), we used the analysis of variance (ANOVA) function aov in the R software package stats. We included the interaction between sampling period and region as the independent variable, to account for environmental variability among regions while testing for temporal variation in dependent variables. We used redundancy analysis (RDA) to characterize environmental controls on carbon cycling across our study regions. Dependent variables in the RDA included measurements of gas efflux ( $J_{\rm CO2}$  and  $J_{\rm CH4}$ ) and carbon yields (DIC, PIC, DOC, and POC). Explanatory (environmental) variables included water quality and chemistry (water temperature, specific conductance, dissolved oxygen, pH, d-excess, and TDN yield) and landscape conditions (terrain slope, GPP, SOC 0-100 cm), percent distribution of surficial geology units (carbonate, colluvial, moraine, and organic), and lake coverage. The RDA used mean summertime values from the 18 of 33 sites for which all carbon species were measured. Prior to performing the RDA, values were log or square root transformed to achieve normality. To simplify the RDA, we performed automated stepwise model selection using the *ordistep* function from the R package *vegan* (Oksanen et al., 2018). To determine potential contributions from pluvial events to variation in stream chemistry and constituent export (Beel et al., 2021; Kokelj et al., 2015), we tested correlations between rainfall, stream chemistry, and total carbon export. Using data from the meteorological station nearest each region (Figure 1), we calculated total rainfall at 0, 12, 24, 48, 72, and 96 hr prior to sample collection at each site to test for immediate and delayed effects from rainfall on stream flow and constituent transport. Unless noted, values for individual sites are reported as summertime mean  $\pm$  standard error, values for study regions (n = 4) are reported as the

ZOLKOS ET AL. 7 of 21

means of individual sites  $\pm$  standard error, and values across all sites (n = 33) as mean  $\pm$  one standard deviation (1 $\sigma$ ). Additional information is available in Supporting Information S1.

#### 3. Results

### 3.1. Physiographic and Meteorological Conditions Underlying Regional Ecosystem Variation

Physiographic and meteorological characteristics varied considerably among study regions (Table 1). These varied conditions in part underlie regional variation in hydrology. Runoff was highest on the Peel Plateau (4.5 mm d<sup>-1</sup>), where total summertime precipitation was highest (238 mm), intermediate in the Richardson Mountains (2.6 mm d<sup>-1</sup>), and lowest in the low-relief Mackenzie Lowlands and Travaillant Uplands (both ~0.5 mm d<sup>-1</sup>). In the Mackenzie Lowlands and Travaillant Uplands, where lakes and ponds covered 7%–18% of the study watersheds (Table S3 in Supporting Information S1), lower d-excess values represented deviation from the global meteoric water line and stronger effects from evaporation on regional hydrology (Table S3 in Supporting Information S1).

#### 3.2. Stream Water Quality and Chemistry

Specific conductance was higher in streams in the previously unglaciated Richardson Mountains (mean = 225  $\mu$ S cm<sup>-1</sup>) than those in the ice-rich moraine Peel Plateau (149  $\mu$ S cm<sup>-1</sup>), poorly drained Mackenzie Lowlands (95  $\mu$ S cm<sup>-1</sup>), and rolling till plains of the Travaillant Uplands (82  $\mu$ S cm<sup>-1</sup>). Temperatures were lower and dissolved oxygen levels higher in streams of the Richardson Mountains (5.6°C, 11.0 mg L<sup>-1</sup>) and Peel Plateau (7.1°C, 11.1 mg L<sup>-1</sup>) than in those of the Travaillant Uplands (11.6°C, 8.6 mg L<sup>-1</sup>) and Mackenzie Lowlands (13.0°C, 9.9 mg L<sup>-1</sup>). On average, pH was lower on the Peel Plateau (5.31) than in the other regions (6.65–6.86) (Table 2). Weathering ions plotted using a Piper diagram showed that all streams were characterized by Ca<sup>2+</sup>-Mg<sup>2+</sup> type waters, with varying contributions from H<sub>2</sub>CO<sub>3</sub> versus sulfuric acid (H<sub>2</sub>SO<sub>4</sub>) driven carbonate weathering (Figure 2).

DOC was the primary carbon species in the Mackenzie Lowlands (1,900 µM) and Travaillant Uplands (1,510 µM), where organic surficial deposits were abundant (Table S3 in Supporting Information S1), and SOC and GPP were higher (Table 1). Across sites, DOC concentrations were strongly anticorrelated with mean watershed elevation  $(p_{31} < 0.001, R^2 = 0.79)$ . DIC concentrations in streams of the Richardson Mountains (1,816  $\mu$ M) were two to six times higher than in the other regions and comprised primarily of  $HCO_3^-(1,730~\mu\text{M})$ . Because pH among all sites was circumneutral to acidic,  $CO_3^{2-}$  was a minor component of DIC ( $\leq 0.3\%$ ). Concentrations of POC were relatively low for most regions (24-99 µM) except the Peel Plateau (2,483 µM), where the highest POC concentrations were observed in with streams affected by hillslope RTS activity. Our analysis of 36 total PC samples from the Peel Plateau allowed for an estimate of a mean PIC:POC ratio of 0.15. We acknowledge that this ratio developed using suspended solids from Peel Plateau streams may vary in other regions due to, for instance, particulate composition. However, use of these ratios enables first-order estimates of total carbon and the carbon balance in a region where this has not been previously examined (Methods S4 in Supporting Information S1). Total dissolved and PC concentrations (Σ[DIC, PIC, DOC, and POC]) were highest and most variable in streams of the Peel Plateau (4,400 µM) (Table 2). Excluding RTS-affected streams, however, mean concentrations were slightly lower on the Peel Plateau (1,360 μM) (Table S4 in Supporting Information S1) than in the other regions  $(1,770-4,210 \mu M)$ .

Across all study sites,  $\delta^{13}\text{C-DIC}$  (-13.0%  $\pm 4.4\%$ ) showed relatively greater variation than  $\delta^{13}\text{C-DOC}$  (-27.3%  $\pm 0.3\%$ ),  $S_R$  ( $0.85 \pm 0.05$ ), and SUVA<sub>254</sub> ( $3.77 \pm 0.58$  L mgC<sup>-1</sup> m<sup>-1</sup>), and thus provided more utility in discerning carbon sources and cycling. The span of  $\delta^{13}\text{C-DIC}$  values occurred across a large pH gradient, with paired values reflective of fractionation more strongly coupled to biotic production and atmospheric exchange of CO<sub>2</sub> at lower pH, and increasing contributions from primarily  $H_2\text{CO}_3$  and/or  $H_2\text{SO}_4$  carbonate weathering at higher pH (Figure 3). On the Peel Plateau,  $\delta^{13}\text{C-DIC}$  was generally lower in non-RTS affected headwaters (PP-7 = -23.4%) than in larger RTS-affected watersheds (PP-8 = -5.9%). In the high pH streams of the Richardson Mountains, relatively constrained  $\delta^{13}\text{C-DIC}$  values (-8.3% to -11.7%) aligned with DIC sourced primarily from carbonate weathering, whereas lower values in the Mackenzie Lowlands (-9.5% to -17.5%) and Travaillant Uplands (-6.1% to -18.4%) were indicative of biotic CO<sub>2</sub> comprising a larger portion of DIC (Figure 3). Stronger biotic CO<sub>2</sub> production in the Mackenzie Lowlands was also evidenced by pCO<sub>2</sub> and pCH<sub>4</sub> that were, on average, more than 30% higher than in the other regions (Table 2).

ZOLKOS ET AL. 8 of 21

 Table 2

 Water Quality, Chemistry, and Carbon Fluxes in Streams of the Western Canadian Arctic

Parameter	Units	Richardson Mountains	Peel Plateau	Mackenzie Lowlands	Travaillant Uplands					
Water quality and chemistry										
Temperature	°C	5.6 (0.6)	7.1 (0.7)	13.0 (0.6)	11.6 (0.6)					
Sp. conductance	$\mu S cm^{-1}$	255 (51)	149 (76)	95 (13)	82 (7)					
Dissolved oxygen	${\rm mg}~{\rm L}^{-1}$	11.0 (0.3)	11.1 (0.4)	8.6 (0.7)	9.9 (0.7)					
pH	pH units	6.86 (0.4)	5.31 (0.4)	6.68 (0.2)	6.65 (0.2)					
DOC	μΜ	325 (75)	1,051 (198)	1,899 (303)	1,507 (104)					
DIC	$\mu M$	1,816 (456)	298 (102)	776 (85)	578 (39)					
POC	$\mu M$	24 (8)	2,483 (1,654)	56 (16)	99 (62)					
PIC	μΜ	4 (1)	382 (255)	9 (2)	15 (10)					
TC	$\mu M$	3,268 (174)	4,389 (1,973)	2,948 (383)	2,171 (244)					
$p\mathrm{CO}_2$	μatm	1,300 (202)	1,537 (326)	2,700 (681)	1,592 (381)					
$p\mathrm{CH}_4$	μatm	102 (55)	309 (93)	341 (56)	243 (97)					
CO <sub>2</sub> excess	-	3.5 (0.3)	4.1 (0.5)	6.7 (1.1)	3.3 (0.5)					
CH <sub>4</sub> excess	-	106 (73)	178 (52)	216 (35)	135 (55)					
TDN	$\mu M$	18.4 (1.4)	29.4 (5.1)	52.4 (5.8)	37.0 (4.4)					
DIN	$\mu M$	6.2 (1.7)	6.9 (3.3)	1.3 (0.2)	2.8 (1.2)					
$NH_4^+$	$\mu M$	0.1 (0.02)	4.2 (1.2)	0.9 (0.1)	2.2 (0.8)					
$NO_3^-$	$\mu M$	6.1 (1.3)	1.8 (0.6)	0.3 (0.2)	0.7 (0.2)					
$\delta^{13}$ C-DIC	% <sub>o</sub> VPDB	-9.8 (0.9)	-14.8 (2.4)	-13.4 (1.4)	-13.7 (1.9)					
$\delta^{13}$ C-DOC	%eVPDB	-27.3 (0.0)	-27.1 (0.1)	-27.5 (0.1)	-27.4 (0.0)					
d-excess	-	7.0 (0.3)	8.7 (0.1)	-1.3 (1.6)	1.4 (1.7)					
Water and carbon flux	xes									
DOC flux	$\rm mmol~s^{-1}$	104 (55)	139 (105)	463 (180)	695 (445)					
DIC flux	$\rm mmol~s^{-1}$	1,219 (735)	100 (98)	296 (167)	289 (189)					
POC flux	$\rm mmol~s^{-1}$	7.7 (3.1)	1,127 (908)	18.3 (6.2)	52 (40)					
PIC flux	$\rm mmol~s^{-1}$	1.2 (0.5)	174 (131)	2.8 (1.0)	8.0 (6.2)					
TC flux	$\rm mmol~s^{-1}$	1,070 (630)	1,643 (1,544)	1,037 (620)	1,321 (881)					
DOC yield	$\mu mol \; m^{-2} \; d^{-1}$	949 (327)	4,812 (1,672)	1,040 (355)	754 (123)					
DIC yield	$\mu mol \; m^{-2} \; d^{-1}$	3,453 (865)	984 (186)	408 (105)	275 (39)					
POC yield	$\mu mol \; m^{-2} \; d^{-1}$	38 (9)	5,801 (3,515)	37 (9)	43 (22)					
PIC yield	$\mu mol \; m^{-2} \; d^{-1}$	5.9 (1.5)	893 (541)	5.7 (1.4)	6.6 (3.4)					
TC yield	$\mu mol \; m^{-2} \; d^{-1}$	5,777 (1,465)	12,715 (4,178)	2,068 (636)	1,188 (187)					
$J_{ m CO2}$	$\mu mol \; m^{-2} \; s^{-1}$	4.3 (0.6)	3.7 (1.0)	5.6 (0.8)	4.2 (1.4)					
$J_{ m CH4}$	nmol $m^{-2}$ $s^{-1}$	32.4 (18.2)	46.0 (14.4)	24.7 (4.3)	19.0 (4.4)					
$k_{\rm CO2}$	$m d^{-1}$	7.8 (0.9)	5.6 (0.7)	6.0 (0.9)	6.5 (1.1)					
$k_{\mathrm{CH4}}$	$m d^{-1}$	172 (151)	15.1 (5.3)	8.7 (2.7)	9.9 (2.3)					
Q	$m^3\;s^{-1}$	0.52 (0.31)	0.16 (0.10)	0.33 (0.16)	0.53 (0.35)					
Runoff	mm d <sup>-1</sup>	2.6 (0.5)	4.5 (0.9)	0.5 (0.1)	0.5 (0.1)					

*Note.* Values are regional mean  $\pm$  standard error during the summertime study period. See Table S4 in Supporting Information S1 for mean  $\pm$  standard error for each site. TC = total carbon ( $\Sigma[IC, OC]$ ).

ZOLKOS ET AL. 9 of 21

wiley.com/doi/10.1029/2022GB007403 by University Of Alaska Fairbanks, Wiley Online Library on [17/02/2023]. See the Terms and Conc

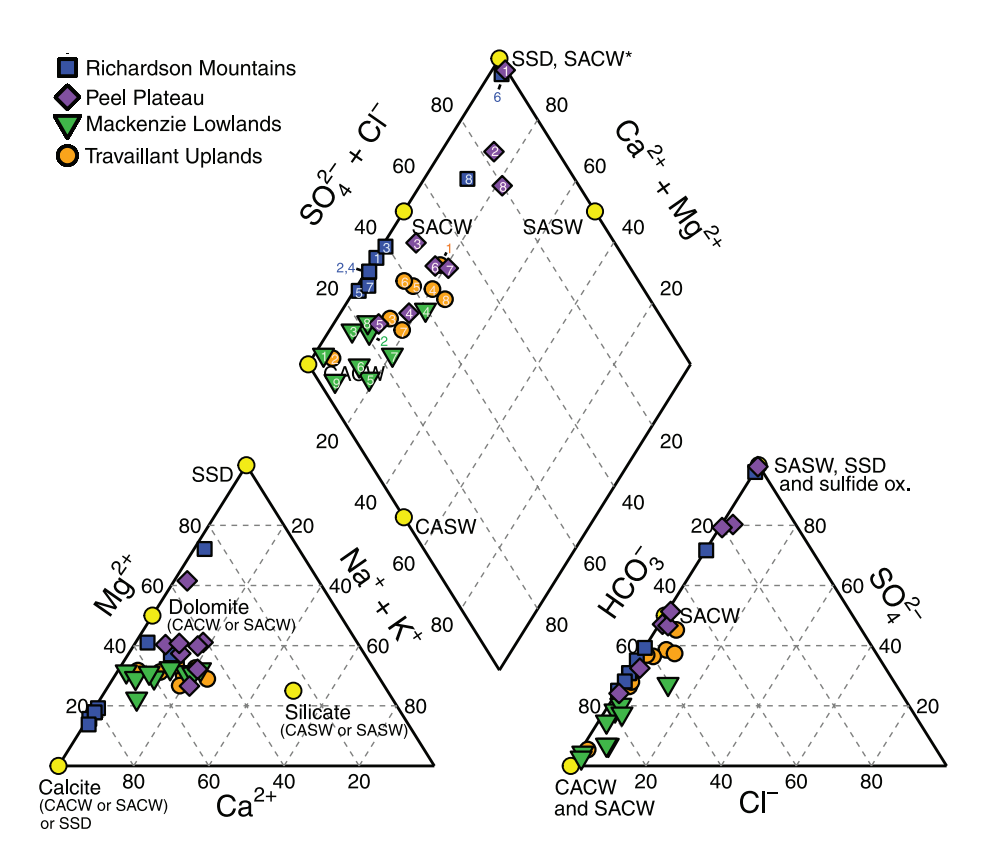


Figure 2. Piper diagram showing stream geochemistry as proportions of ion equivalent concentrations for the four study regions: Richardson Mountains (previously unglaciated), Peel Plateau (ice-rich tills), Mackenzie Lowlands (organic-rich), and Travaillant Uplands (rolling till plains). CACW =  $H_2CO_3$  carbonate weathering, SACW =  $H_2CO_3$  carbonate weathering, CASW =  $H_2CO_3$  silicate weathering, SASW =  $H_2CO_3$  silicate weathering, and SSD = sulfate salt (gypsum) dissolution. End members determined from equations in the text. Site numbers shown within symbols of upper diamond plot.

TDN was lowest in the Richardson Mountains (18  $\mu$ M), intermediate on the Peel Plateau (29  $\mu$ M) and in the Travaillant Uplands (37  $\mu$ M), and highest in the Mackenzie Lowlands (52  $\mu$ M) and, on average, comprised of 85% DON. Similar to DOC, SOC, and GPP, TDN was anticorrelated with mean watershed elevation ( $p_{18} < 0.001$ ,  $R^2 = 0.85$ ). DIN was highest on the Peel Plateau (6.9  $\mu$ M) and in the Richardson Mountains (6.2  $\mu$ M), and lower in the Travaillant Uplands (2.8  $\mu$ M) and Mackenzie Lowlands (1.3  $\mu$ M). DIN was primarily NH<sub>4</sub><sup>+</sup> except in the Richardson Mountains, where DIN was primarily NO<sub>3</sub><sup>-</sup> (Table 2).

## 3.3. Fluvial Carbon Fluxes in Total and by Species

Lateral fluvial carbon fluxes ( $\Sigma[\mathrm{DIC},\mathrm{PIC},\mathrm{DOC},\mathrm{and}\,\mathrm{POC}]$ ) were largest and most variable on the Peel Plateau (1,643  $\pm$  1,544 mmol s<sup>-1</sup>), and smallest and least variable in the Mackenzie Lowlands (1,037  $\pm$  620 mmol s<sup>-1</sup>) (Table 2). The ANOVA revealed no temporal variation in constituent concentrations or lateral fluxes during the summer sampling period (Table S5 in Supporting Information S1). Excess  $\mathrm{CO}_2$  (range = 3.3–6.7) and  $\mathrm{CH}_4$  (106–216) substantially greater than one indicated  $\mathrm{CO}_2$  and  $\mathrm{CH}_4$  efflux to the atmosphere, which was corroborated and quantified by direct measurements (Table 2, Table S4 in Supporting Information S1). Broadly,  $\mathrm{CO}_2$  efflux trended opposite elevation and relief. Mean  $J_{\mathrm{CO}2}$  was highest in the low-relief, organic-rich Mackenzie Lowlands (5.6  $\mu$ mol m<sup>-2</sup> s<sup>-1</sup>) and lowest on the Peel Plateau (3.7  $\mu$ mol m<sup>-2</sup> s<sup>-1</sup>). Rates of  $\mathrm{CO}_2$  transfer were, on average, higher in the Richardson Mountains ( $k_{\mathrm{CO}2}$  = 7.8 m d<sup>-1</sup>) than in the other regions (5.6–6.4).  $J_{\mathrm{CH}4}$  was higher and more variable in the relatively high-velocity streams on the Peel Plateau (46.0 nmol m<sup>-2</sup> s<sup>-1</sup>) and Richardson Mountains (32.4 nmol m<sup>-2</sup> s<sup>-1</sup>), where  $k_{\mathrm{CH}4}$  was also high and variable (mean for both regions = 93.6 m d<sup>-1</sup>) (Table 2).

The proportional fluxes of individual carbon species (p) illustrate how the types of carbon comprising total fluvial carbon flux (lateral plus efflux) varied among regions. Mean proportional fluxes were generally highest

ZOLKOS ET AL. 10 of 21

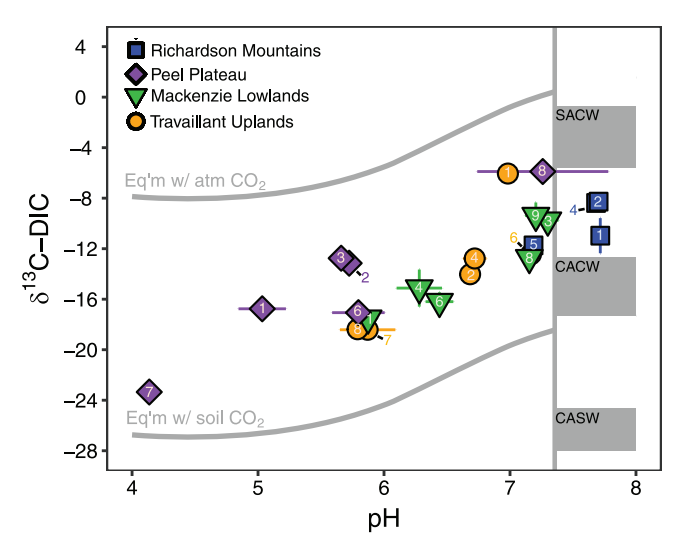


Figure 3. Composition of stable dissolved inorganic carbon isotopes  $(\delta^{13}\text{C-DIC})$  versus pH among the four study regions: Richardson Mountains (previously unglaciated), Peel Plateau (ice-rich tills), Mackenzie Lowlands (organic-rich), and Travaillant Uplands (rolling till plains). Mean values are shown with error bars representing range. In some cases, error bars are smaller than the symbol (n = 2 for most points). Curvilinear reference lines depict theoretical end-members for equilibrium reactions with atmospheric and biogenic CO<sub>2</sub>. Gray areas span theoretical end-member values for kinetically controlled mineral weathering reactions. SACW = H<sub>2</sub>SO<sub>4</sub> carbonate weathering;  $CACW = H_2CO_3$  carbonate weathering;  $CASW = H_2CO_3$  silicate weathering. Site numbers shown within symbols. The vertical lines assists in visually distinguishing the pH at which <10% of DIC is comprised of CO<sub>2</sub> and thus kinetic reactions (weathering end-members) are inferred to have greater effects on stable isotope values than equilibrium reactions.  $\delta^{13}$ C-DIC values are reflective of isotope fractionation more strongly coupled to biotic production and atmospheric exchange of CO2 at lower pH, and increasing contributions from primarily H2CO3 and/or H2SO4 carbonate weathering at higher pH.

for DOC (DOC<sub>p</sub> = 0.11-0.51), DIC (0.10-0.74), and  $J_{CO2}$  (0.10-0.29) (Figure 4a, Table S6 in Supporting Information S1). In the colluviated Richardson Mountains, DIC comprised the largest proportion of total carbon flux (0.74), whereas carbon fluxes on the Peel Plateau were mostly DOC (0.46) and POC (0.29). On the Peel Plateau, lateral fluxes of POC in RTS-affected streams were roughly 10 times larger than in pristine streams and comprised 66%-69% of the total fluvial carbon flux. DOC was the largest flux component in the organic-rich Mackenzie Lowlands (0.48) and Travaillant Uplands (0.51), followed by  $J_{\rm CO2}$  (~0.26) and DIC (~0.20). These proportional fluxes together with daily lateral fluvial carbon yields reinforced patterns in carbon cycling coupled to physiographic variation across study regions. In the Richardson Mountains, lateral yields across sites were moderate (5,800 µmol m<sup>-2</sup> d<sup>-1</sup>) and almost entirely comprised of DIC (66%) and DOC (13%). DIC yields were lower relative to runoff where silicate lithologies predominated (RM-6-8, PP-1-7), and higher where carbonate bedrock (RM-1-5) and RTS-activity (PP-8) were widespread (Figure 4b). On average, lateral yields for two RTS-affected watersheds (PP-2 and PP-8) on the Peel Plateau (20,300 μmol m<sup>-2</sup> d<sup>-1</sup>) were more than five times higher than at all other sites (Table S4 in Supporting Information S1). This was primarily due to POC release, yet among all sites there were no clear trends between POC yield and runoff because disturbance effects overwhelmed other sources of between-catchment conditions (Figure 4d). In the Mackenzie Lowlands and Travaillant Uplands, organic carbon comprised more than 75% of the lateral yields. The relationship between dissolved carbon yields and runoff was similar for these two regions. Specific conductance, but not total carbon export, showed moderate albeit significant correlation with prior rainfall at several intervals for sites in the Richardson Mountains and Travaillant Uplands (Figures S1 and S2 in Supporting Information S1).

#### 3.4. Multivariate Indicators of Regional Patterns in Carbon Cycling

Simultaneously evaluating carbon yields and geospatial metrics of physiographic conditions refined understanding of the associations between carbon cycling and regional environmental characteristics. The trimmed

RDA retained significant variables for water quality, nutrients, and landscape factors (Table 3). The ANOVA revealed no temporal variation in these variables during the summer sampling period, except for GPP (Table S5 in Supporting Information S1), which decreased from June to August. RDA axis one (RDA1) and two (RDA2) were both significant. Broadly, RDA1 separated carbon export among gaseous, dissolved, and PC species. Most sites in the lake- and organic-rich Mackenzie Lowlands and rolling till plains of the Travaillant Uplands plotted in a cluster of negative values along RDA1, and were associated with more organic carbon (SOC), higher vegetation productivity (GPP), and higher CO<sub>2</sub> and CH<sub>4</sub> efflux (Figure 5). On the Peel Plateau, RTS-affected sites two and eight plotted with high RDA1 values and were associated with PC export. While RDA1 separated among carbon species, RDA2 was associated with regional differences in terrain relief and carbon accumulation. Along RDA2, sites in the southern Richardson Mountains were associated with higher DIC yields, specific conductance, and carbonate coverage, reflecting more intense physical erosion and chemical weathering of carbonate bedrock.

# 3.5. Fluvial Carbon Fluxes Relative to Net Ecosystem Exchange

Modeled estimates of NEE from SPL4CMDL ranged from -0.60 gC m<sup>-2</sup> d<sup>-1</sup> in the Travaillant Uplands to -0.82 gC m<sup>-2</sup> d<sup>-1</sup> in the Mackenzie Lowlands (Table 1). Estimated for the entire fluvial network in each watershed, upscaled fluvial effluxes of CO<sub>2</sub> and CH<sub>4</sub> were, on average, equivalent to 2% of NEE and total lateral carbon fluxes were, on average, 15% of NEE (Figure 6, Table S6 in Supporting Information S1). Considering all carbon species, total fluvial carbon flux ( $\Sigma[J_{CO2}, J_{CH4}, DIC, DOC, PIC, and POC]$ ) across regions was equivalent to 17% of NEE (range = 4%–59%). Among regions, total fluvial carbon flux relative to NEE was lowest in the Travaillant

ZOLKOS ET AL. 11 of 21

19449224, 2022, 9, Downloa

elibrary.wiley.com/doi/10.1029/2022GB007403 by University Of Alaska Fairbanks, Wiley Online Library on [17/02/2023]. See the Terms

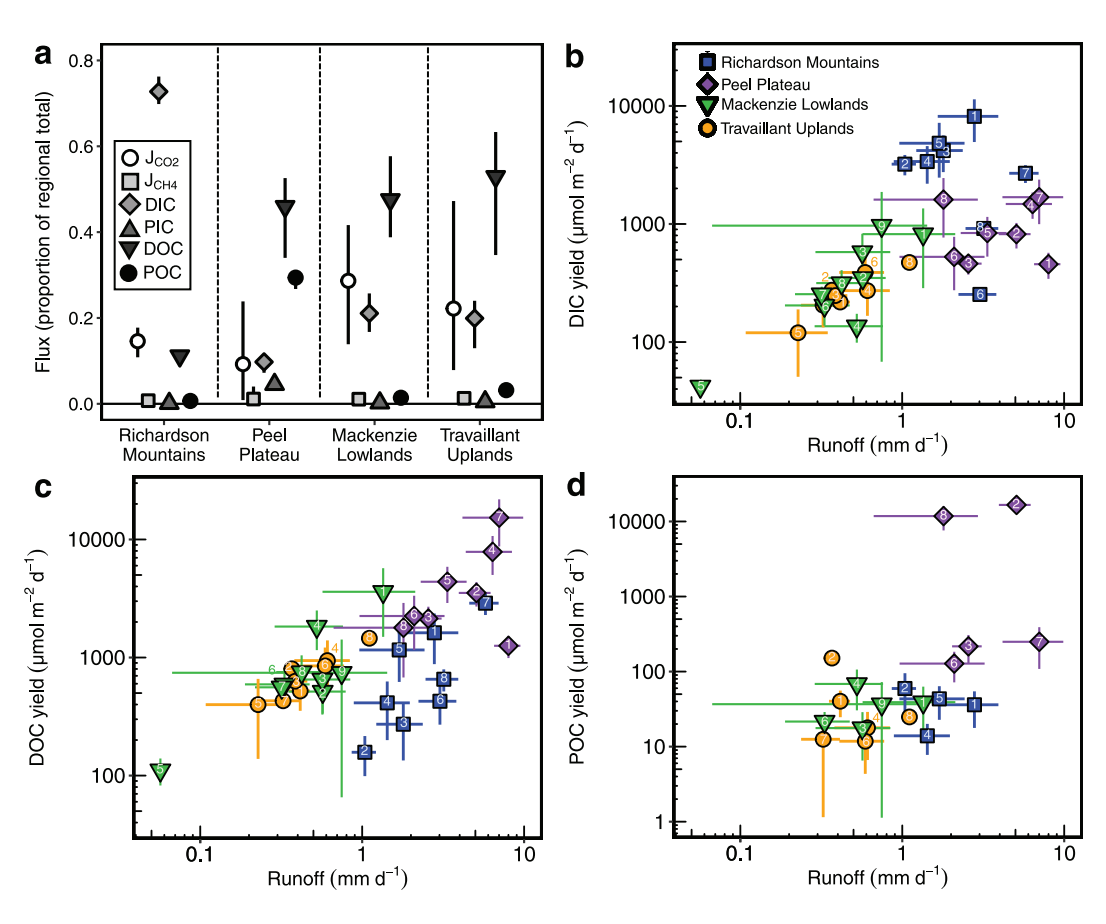


Figure 4. Carbon fluxes and yields among the four study regions: Richardson Mountains (previously unglaciated), Peel Plateau (ice-rich tills), Mackenzie Lowlands (organic-rich), and Travaillant Uplands (rolling till plains). (a) Fluxes (mean  $\pm$  range) of carbon species in each region, shown as a proportion of the total in each region. Yields versus runoff for (b) dissolved inorganic carbon (DIC), (c) dissolved organic carbon (DOC), and (d) particulate organic carbon (POC). For panels (b–d), error bars represent mean  $\pm$  standard error.

Uplands (4%–13%) and Mackenzie Lowlands (5%–15%), where streamflow velocity was lower and GPP was higher, and higher in the Richardson Mountains (11%–25%). Total fluvial carbon fluxes relative to NEE were highest and most variable on the Peel Plateau (8%–59%), due to a first-order watershed with relatively high DOC flux (PP-7) and two RTS-affected watersheds with high lateral carbon fluxes relative to NEE (PP-2 = 52% and PP-8 = 57%) (Table S6 in Supporting Information S1).

# 4. Discussion

## 4.1. Stream Chemistry and Carbon Cycling Are Coupled to Varied Landscape Histories

In the western Canadian Arctic, regional variation in stream water chemistry reveals how geology and climate history since the LGM have shaped the evolution of landscapes along varied trajectories, giving rise to diverse contemporary ecosystems and modes of carbon cycling and defining potential trajectories of future change.

The high-relief Richardson Mountain study sites are beyond the westernmost limit of the LIS and are comprised of ice-poor colluvial slopes and exposed bedrock, resulting in enhanced erosion and chemical weathering. DIC yields in the Richardson Mountain sites alone were double the summed dissolved and PC yields in the Mackenzie Lowlands and Travaillant Uplands. Relatively high pH and stream water specific conductance, trends in major ions (Figure 2), and  $\delta^{13}$ C-DIC values (Figure 3) indicate that DIC in the southern Richardson Mountains sites derives mainly from carbonate weathering by  $H_2$ CO<sub>3</sub>, likely from atmospheric CO<sub>2</sub> dissolved within summertime rainfall and from minor contributions of organic acids from GPP within this relatively sparsely vegetated landscape. Sulfide oxidation and/or sulfate salt dissolution were most strongly indicated in the subset

ZOLKOS ET AL. 12 of 21

19449224, 2022, 9, Downloaded from http:

**Table 3**Summary of the Significance of Landscape Covariates and Axes From the Redundancy Analysis (RDA) of Carbon Export, Stream Chemistry, and Landscape Characteristics

	df	p	F	Variance
Covariate				
pН	1	< 0.01	52.1	4.61
Carbonate (%)	1	< 0.01	27.2	2.41
Dissolved oxygen (%)	1	< 0.01	14.3	1.27
Sp. conductance	1	< 0.01	14.0	1.24
d-excess	1	0.01	7.7	0.68
TDN yield	1	0.02	6.4	0.57
Lakes/ponds (%)	1	0.02	5.5	0.49
SOC	1	0.02	5.3	0.47
Organic (%)	1	0.03	4.7	0.42
Slope	1	0.07	3.3	0.29
GPP	1	0.25	1.5	0.13
Residual	6	-	-	0.53
RDA axis				
RDA1	1	< 0.01	206.0	9.12
RDA2	1	< 0.01	43.5	1.93
RDA3	1	0.05	17.6	0.78
RDA4	1	0.34	14.9	0.66
RDA5	1	0.99	2.0	0.09
Residual	12	-	_	0.53

of watersheds in the Richardson Mountains containing shale lithologies (RM-6 and RM-8). High DIC yields and low DOC yields relative to runoff (Figures 4b and 4c) further emphasize relatively stronger contributions from mineral weathering to carbon cycling in the southern Richardson Mountains than in the other regions. While climate warming and permafrost thaw may not manifest in the Richardson Mountains as thaw-induced mass wasting as occurring on the ice-rich Peel Plateau, biogeochemical effects may be stark nonetheless: an increase in atmospheric CO<sub>2</sub> from 355 to 560 ppm is predicted to increase CO<sub>2</sub> drawdown by 50% via enhanced H<sub>2</sub>CO<sub>3</sub> carbonate and silicate weathering in the Richardson Mountains and elsewhere across the Mackenzie River Basin (Beaulieu et al., 2012). This enhanced weathering would contribute to a 18% increase in HCO<sub>3</sub> export from the Mackenzie River to the coastal Arctic Ocean, which could help to counterbalance future increases in ocean acidification associated with increasing riverine organic carbon export (Tank et al., 2012; Terhaar et al., 2019). This estimate does not account for thermokarst in watersheds of major tributaries like the Peel, where intensifying hillslope thermokarst is driving increased carbonate alkalinity concentrations and export through fluvial networks (Tank et al., 2016; Zolkos et al., 2020).

In contrast to the colluviated Richardson Mountains, intensifying thaw-driven mass wasting of ice-rich moraine deposits on the Peel Plateau enhances chemical weathering of carbonates, and fluvial fluxes of  $HCO_3^-$  and particulates relative to non-RTS affected streams. Indeed, relatively high specific conductance and total carbon yields in streams on the Peel Plateau were driven by hillslope RTS-affected sites PP-2 and PP-8. Major ions and  $\delta^{13}$ C-DIC show that fluvial DIC in Peel Plateau streams originates mainly from  $H_2SO_4$  carbonate weathering—which is a  $CO_2$  source over geological timescales (Calmels et al., 2007)—with some biotic  $CO_2$  indicated by relatively depleted  $\delta^{13}$ C-DIC values. The signal of  $H_2SO_4$  carbonate weathering was strongest for site PP-8, which integrates biogeochemical effects of multi-

ple large hillslope RTSs. This aligns with the understanding that growth of RTSs on the Peel Plateau can mobilize increasingly greater quantities of deeper carbonate- and sulfide-bearing permafrost till to chemical weathering fronts (Kokelj et al., 2021; Zolkos et al., 2018). Our RDA further reveals that RTS activity shifts fluvial networks from conveyors of primarily dissolved carbon to PC (sites PP-2 and PP-8 in Figure 5) (Littlefair et al., 2017; Shakil et al., 2020). RTS-enhanced sediment and PC export on the Peel Plateau, observed in this and other studies (Kokelj et al., 2013; Shakil et al., 2020), is reflected in the orders of magnitude higher PC yields in RTS-affected sites PP-2 and PP-8 (Figure 4d).

Despite striking mobilization of permafrost carbon via hillslope thermokarst, the high rates of CH<sub>4</sub> efflux for three sites (PP-4, 5, 6; Table S4 in Supporting Information S1) in low-relief (mean slope =  $2.8^{\circ}$ ) and relatively organic-rich watersheds (mean DOC =  $1,200 \,\mu\text{M}$ ) on the Peel Plateau highlights variation in carbon cycling even within the varied regions along our transect. Similar observations on the Peel Plateau and elsewhere indicate that spatial variability in the accumulation of organics is a primary driver of CH<sub>4</sub> production and efflux (Crawford et al., 2017; Zolkos et al., 2019). The negative correlation between  $p\text{CH}_4$  and  $\text{NO}_3^-$  ( $p_{18} < 0.001, R^2 = 0.52$ ), as well as  $p\text{CH}_4$  and  $\text{SO}_4^{2-}$  ( $p_{31} < 0.001, R^2 = 0.68$ ), indicates suppression of methanogenesis across regions, due to the presence of alternative electron acceptors that microbes use preferentially (Bridgham et al., 2013; Schädel et al., 2016).

In contrast to the Richardson Mountains and Peel Plateau, the Mackenzie Lowlands and Travaillant Uplands displayed starkly different aquatic environments and modes of fluvial carbon cycling. Stream temperatures and dissolved oxygen levels reflected warmer, less oxygenated conditions across these peatland-dominated and relatively lake-rich low-relief landscapes. Ions indicate that carbonate weathering also generated DIC in the Mackenzie Lowlands, but lower  $\delta^{13}$ C-DIC values suggest this weathering was more strongly coupled to  $H_2CO_3$  production from soil organic matter oxidation within the abundant peatlands and plant root respiration (Berner, 1992)

ZOLKOS ET AL. 13 of 21

19449224, 2022, 9, Downloaded from http:

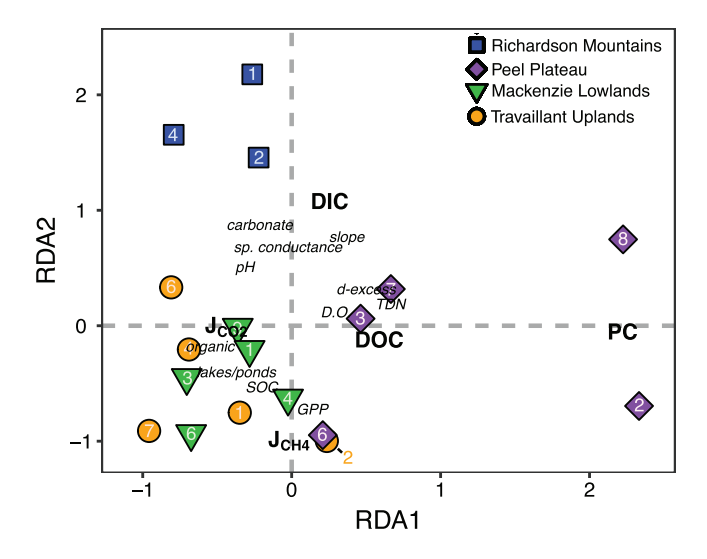


**Figure 5.** Ordination plot of redundancy analysis of mean summertime carbon yields (bold text) and landscape and water chemistry variables (italicized) among the four study regions: Richardson Mountains (previously unglaciated), Peel Plateau (ice-rich tills), Mackenzie Lowlands (organic-rich), and Travaillant Uplands (rolling till plains). Site numbers shown within points (Figure 1, Table S1 in Supporting Information S1). Peel Plateau sites 2 and 8 were downstream of active retrogressive thaw slump thermokarst features. DOC = dissolved organic carbon. PC = particulate organic and inorganic carbon.  $J_{\rm CO2}$  and  $J_{\rm CH4}$  = CO<sub>2</sub> and CH<sub>4</sub> efflux. D.O. = dissolved oxygen. TDN = total dissolved nitrogen yield. Sp. conductance = specific conductance. GPP = mean watershed gross primary productivity. SOC = mean watershed soil organic carbon content at 1 m depth. Slope = mean watershed slope. Carbonate, colluvial, organic, and lakes/ponds = mean watershed percent coverage of landscape surface types. See units and details in text and Table 1

associated with relatively high vegetation productivity (i.e., GPP). Biotic contributions to the DIC pool were also indicated by high concentrations of DOC, pCO $_2$ , TDN, and SOC, and also by  $\delta^{13}$ C-DOC values (Table 1) similar to  $\delta^{13}$ C of organic carbon in boreal and tundra soils (e.g., Bird et al., 2002; Hicks Pries et al., 2013), which together indicate that soil-stream linkages (e.g., Campeau et al., 2018) drive summertime carbon cycling in the poorly drained, organic-rich Mackenzie Lowlands. Lower Q and more negative d-excess values (reflecting greater evaporation) in the Mackenzie Lowlands are reflective of slower-moving water with longer residence times than in the high-relief fluvial networks of the Richardson Mountains and on the Peel Plateau. Longer water residence times in this relatively organic- and lake-rich wetland terrain likely enhanced carbon degradation, contributing to pCO $_2$  and pCH $_4$  supersaturation and a diffusion gradient supportive of the high aquatic CO $_2$  and CH $_4$  efflux we observed (e.g., Rocher-Ros et al., 2019).

Similar to the Mackenzie Lowlands, stream chemistry in the relatively lakeand organic carbon-rich Travaillant Uplands indicated that carbon cycling was driven by biotic processes. However, compared with the Mackenzie Lowlands, the lower SOC and low abundance of carbonate lithologies coupled with low runoff suggest that interactions between terrestrial carbon and flowing waters are relatively more limited in this terrain, as also reflected by the lower sum of dissolved plus PC concentrations (Table 1) and yields (Table S4 in Supporting Information S1). Over millennia, low topographic gradients within these poorly drained permafrost landscapes has favored the accumulation of organics, leading to the development of organic- and nutrient-rich soils and freshwaters that may become a net source of carbon to the atmosphere as the climate warms at northern high latitudes (Hugelius et al., 2020).

# **4.2.** Regional Fluvial Carbon Export and Contributions to Ecosystem Carbon Balance

The distinct ecosystems and associated modes of summertime carbon cycling that have emerged during the Holocene in the western Canadian Arctic

(Section 4.1) underlie regional variation in aquatic carbon export and contributions to ecosystem carbon balance. In the Mackenzie Lowlands and Travaillant Uplands, our finding that lateral transport of DOC and biogenic CO<sub>2</sub> efflux accounted for most of the fluvial carbon flux supports our hypothesis that carbon export would be dominated by organic species in these relatively low-relief, organic- and lake-rich terrains (Figure 4a). In these regions, SOC accumulation and microbial oxidation of organic carbon appear to drive carbon cycling and linkages across the terrestrial aquatic interface (Campeau et al., 2019). Despite this, lower runoff imposed by a shallow terrain gradient (Figure 1) reduces lateral export in these lowland regions compared with the Peel Plateau, where higher runoff mobilizes more organic substrate into fluvial networks (Figures 4c and 4d). While rainfall is known to significantly increase constituent export on the Peel Plateau (Kokelj et al., 2015) and in other permafrost terrains (Beel et al., 2021), we found no strong or consistent effects on stream chemistry or constituent export from rainfall prior to our stream sampling, perhaps because our sampling did not target the largest rainfall events (Figures S1 and S2 in Supporting Information S1). Thus, our estimates of constituent export are likely more conservative than if we had captured rainfall effects with targeted high-frequency sampling. Increased future rainfall at northern high latitudes (Bintanja & Andry, 2017) may partly alleviate hydrologic limitations to carbon export in regions where thaw does not temporarily enhance runoff (Connon et al., 2021), and prompt further divergence in summertime carbon cycling by enhancing PC export on the Peel Plateau (Kokelj et al., 2015). In the previously unglaciated, sparsely vegetated Richardson Mountains, lower DOC yields at comparable levels of runoff reflect source limitation imposed by sparser terrestrial organic carbon stores. Predominance of DIC yields (mainly as HCO<sub>3</sub><sup>-</sup>) in the Richardson Mountains emphasizes a primarily mineral weathering-driven pathway of atmospheric CO<sub>2</sub> uptake, transfer into fluvial networks, and export to downstream environments. From a climate

ZOLKOS ET AL. 14 of 21

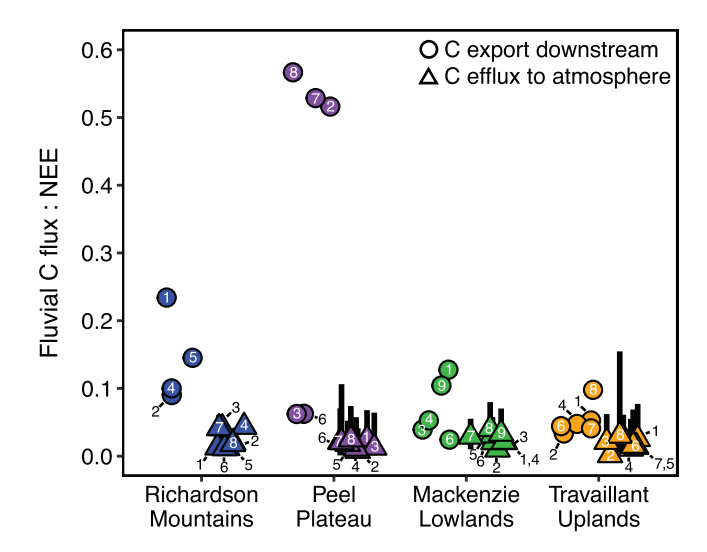


**Figure 6.** The proportion of fluvial carbon flux relative to net ecosystem exchange (NEE) for sites among the four study regions: Richardson Mountains (previously unglaciated), Peel Plateau (ice-rich tills), Mackenzie Lowlands (organic-rich), and Travaillant Uplands (rolling till plains). Values are shown separately for lateral export (circles) and efflux to the atmosphere (triangles). Lateral export represents summed dissolved and particulate inorganic and organic carbon. Efflux to the atmosphere represents summed  $\rm CO_2$  and  $\rm CH_4$  efflux. Efflux was measured at every site in each region, whereas lateral export presented here is limited by the subset of sites at which particulate carbon was measured. Error bars for efflux span the estimated range of fluvial surface area. Error bars for lateral export are smaller than the data points.

perspective, DIC export throughout our study regions and the circumpolar north will continue to represent a  $CO_2$  sink or neutrality where  $H_2CO_3$  rather than  $H_2SO_4$  drives silicate and carbonate weathering (Zolkos et al., 2018).

Contributions from fluvial CO<sub>2</sub> and CH<sub>4</sub> efflux to total fluvial carbon fluxes in the Travaillant Uplands ( $26 \pm 4\%$ , mean  $\pm$  SE) and Mackenzie Lowlands  $(30 \pm 5\%)$  were larger than in the Richardson Mountains  $(11 \pm 5\%)$  and on the Peel Plateau (13  $\pm$  5%). However, we find that CO<sub>2</sub> and CH<sub>4</sub> efflux in the western Canadian Arctic accounts for a smaller proportion of total fluvial carbon fluxes than in the Yukon River basin (~50%) (Striegl et al., 2007, 2012) and in Sweden (58%) (Humborg et al., 2010). Lakes cover 7%–18% of the landscape in the Mackenzie Lowlands and Travaillant Uplands (Table 1). Recent measurements of summertime lacustrine total CH<sub>4</sub> efflux (diffusive plus ebullitive) made in the Mackenzie Lowlands were, on average, 24.7 mgC m<sup>-2</sup> d<sup>-1</sup> (Kuhn et al., 2021). Assuming similar rates of CH<sub>4</sub> efflux from lakes in the Mackenzie Lowlands and Travaillant Uplands during our study period, we estimate that fluvial and lacustrine effluxes would be 32% in the Travaillant Uplands and 48% in the Mackenzie Lowlands. Net CO<sub>2</sub> and CH<sub>4</sub> exchange between lakes and the atmosphere is expected to vary across the northern permafrost region in response to climate warming (Bogard et al., 2019; Walter Anthony et al., 2016) and should be included in future efforts to refine estimates of ecosystem carbon balance.

Our measurements of fluvial carbon flux combined with remote sensing estimates of NEE show that terrestrial productivity in all watersheds assimilated more carbon during the growing season than was lost via efflux and lateral fluxes within fluvial networks. During the shoulder seasons and winter, terrestrial photosynthesis ceases and summertime CO<sub>2</sub> uptake is counterbalanced by CO<sub>2</sub> emissions from ecosystem respiration (Natali

et al., 2019). While not captured by our observations, enhanced terrestrial carbon loss together with aquatic export outside of the growing-season may result in positive NECB annually. Our estimate that total fluvial carbon flux (lateral + efflux) was, on average, equivalent to 6%-38% of carbon uptake by terrestrial vegetation encompasses estimates for the Yukon River basin (14%) (Striegl et al., 2007, 2012), all of Alaska (16%-17%) (McGuire et al., 2018; Stackpoole et al., 2017), and all of Sweden (22%) (Humborg et al., 2010). However, we note that SPL4CMDL NEE, and thus the terrestrial component of our carbon balance assessment, does not include CH<sub>4</sub> exchange, which is typically a net annual source of carbon from northern high latitude terrestrial ecosystems to the atmosphere (Kuhn et al., 2021; Natali et al., 2019). For future studies, we also note that SPL4CMDL estimates of NEE may be more representative of terrestrial CO<sub>2</sub> exchange at multi-kilometer spatial scales similar to the area of the watersheds in this study (mean  $= 50 \text{ km}^2$ ), as indicated by comparison between mean summertime NEE from SPL4CMDL and NEE observed within relatively small footprints of flux towers in boreal and tundra environments (Figure S3 and Table S7 in Supporting Information S1). Importantly, as indicated by this first step toward integrating terrestrial and aquatic carbon fluxes in the western Canadian Arctic presented here, permafrost thaw that manifests as hillslope mass wasting may have significant implications for both aquatic ecosystem function (Chin et al., 2016; Levenstein et al., 2018; Shakil et al., 2021) and ecosystem carbon balance (Song & Wang, 2021).

# 4.3. Intensifying Thaw-Induced Mass Wasting Defines New Trajectories of Permafrost Region Ecosystem Carbon Balance

Regional patterns in fluvial carbon cycling (Section 4.1) and contributions to ecosystem carbon balance (Section 4.2) observed in this study are primarily controlled by ecosystem conditions coupled to variation in geology and topography (RDA2 in Figure 5). These trends are skewed by the distribution of ice-rich till deposits, which are particularly susceptible to climate-driven mass wasting (Kokelj et al., 2021). Although terrains that may be susceptible to thaw-induced mass wasting like hillslope RTSs represent less than 5% of the northern permafrost region (Olefeldt et al., 2016), these thaw features propagate and re-sequester terrestrial carbon across

ZOLKOS ET AL. 15 of 21

increasing watershed scales (Kokelj et al., 2021; Shakil et al., 2020). On the Peel Plateau, RTSs cover <1% of the landscape, but may increase sediment and solute transport by several orders of magnitude (Kokelj et al., 2013; Malone et al., 2013; Zolkos et al., 2020) and enable up to a seven-fold increase in fluvial carbon flux where they occur (see also Shakil et al., 2020). Our measurements of fluvial carbon export on the Peel Plateau offer a striking glimpse of a shifting carbon balance that may come to typify pan-Arctic terrains susceptible to thaw-induced mass wasting. In watersheds directly affected by hillslope RTS, the magnitude of PC export approached 60% of net CO<sub>2</sub> uptake by vegetation (Figure 6 and Table S6 in Supporting Information S1). At a bulk level, POC mobilized by RTS on the Peel Plateau mainly consists of organic matter that is recalcitrant to biotic transformation, including petrogenic organic carbon (Bröder et al., 2021; Keskitalo et al., 2021; Shakil et al., 2021). While erosion of POC and its deposition along the freshwater-to-marine continuum is considered to be an effective mode of carbon sequestration for thousands of years (Goñi et al., 2005; Hilton et al., 2015), the balance between petrogenic oxidation and burial of biogenic organic carbon is important in determining whether the Mackenzie River basin is a net source or sink of carbon to the atmosphere (Horan et al., 2019).

Thermokarst also mobilizes elements other than carbon, as indicated by the elevated concentrations of NH<sub>4</sub><sup>+</sup>, NO<sub>3</sub><sup>-</sup>, and SO<sub>4</sub><sup>2-</sup> observed in this study and elsewhere across the northern permafrost zone (Abbott et al., 2015; Lamhonwah et al., 2017). Complex interactions between carbon and other elemental cycles exist (e.g., Shaver et al., 1992), such as suppression of methanogenesis through the presence of alternate electron acceptors (Bridgham et al., 2013; Schädel et al., 2016), coupling between methanotrophy and nitrogen availability (e.g., Bodelier & Laanbroek, 2004; King, 1997; Liebner & Svenning, 2013), or a general lifting of nutrient limitations leading to stimulation of microbial growth and decomposition even of recalcitrant carbon (Abbott et al., 2015; Voigt et al., 2017; Wild et al., 2014). These linkages between carbon and nutrient cycles are not well studied in Arctic watersheds, but may become increasingly important, especially where intensifying thermokarst activity strengthens land-freshwater linkages (Kokelj et al., 2021).

As thermokarst activity like hillslope RTSs intensify in northwestern Canada (Segal et al., 2016), sediment transport and deposition within fluvial networks (Keskitalo et al., 2021) will likely emerge as a key process of regional ecosystem carbon balance. Our results emphasize that this trajectory of ecosystem carbon balance appears to typify thaw-driven renewal of post-glacial landscape evolution and is therefore likely to emerge in other ice-rich moraine deposits across the circumpolar north (Kokelj, Lantz, et al., 2017). The degree to which this mobilized carbon represents a source of  $\rm CO_2$ —and thus its susceptibility to biogeochemical transformation at a pan-Arctic scale—will influence the strength of the northern high latitude terrestrial carbon sink (Virkkala et al., 2021; Watts et al., 2021) and feedbacks to climate change (Turetsky et al., 2020). Future research priorities should include efforts to: constrain the sources, transformation, and fate of permafrost carbon along the terrestrial-freshwater-marine continuum, particularly in areas susceptible to thaw-induced mass wasting (Keskitalo et al., 2022; Shakil et al., 2022), and integrate terrestrial and aquatic carbon fluxes across permafrost terrains which exhibit varied modes of thaw (e.g., hillslope mass wasting, thermokarst lakes, and active layer deepening), to reduce uncertainty in northern ecosystem carbon balance and the implications for global climate.

# 5. Conclusion

In this study, we investigated how geology together with climate and ecosystem history gave rise to regional variation in present-day fluvial carbon cycling and ecosystem carbon balance in the western Canadian Arctic. We found significant variability in fluvial chemistry and ecosystem carbon balance coupled to diverse biophysical conditions reflected among unglaciated mountains, ice-rich moraine with thaw-driven mass wasting, and organic rich lowlands underlain by glacial tills. In the Richardson Mountains and RTS-affected tributaries of the Peel Plateau, where the exposure of mineral substrate was greatest, mineral weathering was enhanced and abiotic carbon cycling predominated. In the Mackenzie Lowlands and Travaillant Uplands, where low relief has enabled the accumulation of organic matter, hydrochemistry revealed that biotic processes dominated carbon cycling. Across ecoregions, fluvial carbon fluxes in watersheds not affected by thaw-induced wasting were, on average, equivalent to 6%–16% of NEE, and nearly 60% of NEE in watersheds affected by hillslope RTS activity due to amplified lateral carbon export. These results demonstrate that northern permafrost terrains susceptible to thaw-induced mass wasting (Kokelj, Lantz, et al., 2017) may drive emerging trajectories of ecosystem carbon balance, in which the quantity of thawed permafrost carbon mobilized into fluvial networks may be similar in magnitude to carbon uptake by terrestrial vegetation (Plaza et al., 2019). Permafrost thaw and strengthening

ZOLKOS ET AL. 16 of 21

Acknowledgments

Research was supported by the Natural

Sciences and Engineering Research

Council of Canada (Discovery Grant

#430696, Northern Research Supple-

ment #444873), the Campus Alberta

(#617-16), the Colleges and Institutes

Canada (CICan; Clean Tech Intern-

ship #C6134), the UAlberta Northern

of North America Grant-in-Aid. The

Firth, Abraham Snowshoe, Elizabeth

Research Award, and the Arctic Institute

authors thank Lindsey Stephen, Christine

Jerome, and Maya Guttman for assistance

in the field; Shawne Kokelj for providing

meteorological data for the Peel Plateau;

and Anna-Maria Virkkala for insight-

ful conversation about net ecosystem

exchange and carbon balance. Observa-

tions from the Atmospheric Radiation

Measurement (ARM) user facility are

supported by the U.S. Department of

Energy Office of Science managed by the

Program. Work at ANL was supported by

Biological and Environmental Research

the U.S. Department of Energy, Office

Environmental Research, under contract

DE-AC02-06CH11357. The US-Prr and

US-Uaf sites are supported by JAMSTEC

the ArCSII project (JPMXD1420318865).

and IARC/UAF collaboration study and

C. Voigt was supported by the Academy

of Finland project MUFFIN (decision

no. 332196). NWT Geological Survey

contribution 0151.

of Science, Office of Biological and

Innovates Program, the Natural Resources

Canada Polar Continental Shelf Program

terrestrial-freshwater-marine connectivity across the pan-Arctic (Kokelj et al., 2021; Vonk et al., 2019) high-light the need for additional studies which integrate aquatic and terrestrial carbon and nutrient cycling to better constrain ecosystem carbon balance and potential climate feedbacks (Turetsky et al., 2020).

## **Conflict of Interest**

The authors declare no conflicts of interest relevant to this study.

# **Data Availability Statement**

Data used in this study are publicly accessible via Zolkos et al. (2022). Code is available at https://zenodo.org/badge/latestdoi/509124741.

#### References

- Abbott, B. W., Jones, J. B., Godsey, S. E., Larouche, J. R., & Bowden, W. B. (2015). Patterns and persistence of hydrologic carbon and nutrient export from collapsing upland permafrost. *Biogeosciences*, 12(12), 3725–3740. https://doi.org/10.5194/bg-12-3725-2015
- Beaulieu, E., Goddéris, Y., Donnadieu, Y., Labat, D., & Roelandt, C. (2012). High sensitivity of the continental-weathering carbon dioxide sink to future climate change. *Nature Climate Change*, 2(5), 346–349. https://doi.org/10.1038/nclimate1419
- Beel, C. R., Heslop, J. K., Orwin, J. F., Pope, M. A., Schevers, A. J., Hung, J. K. Y., et al. (2021). Emerging dominance of summer rainfall driving High Arctic terrestrial-aquatic connectivity. *Nature Communications*, 12(1), 1448. https://doi.org/10.1038/s41467-021-21759-3
- Berner, R. A. (1992). Weathering, plants, and the long-term carbon cycle. Geochimica et Cosmochimica Acta, 56(8), 3225–3231. https://doi.org/10.1016/0016-7037(92)90300-8
- Bintanja, R., & Andry, O. (2017). Towards a rain-dominated Arctic. *Nature Climate Change*, 7(4), 263–267. https://doi.org/10.1038/nclimate3240 Bird, M., Santrucková, H., Lloyd, J., & Lawson, E. (2002). The isotopic composition of soil organic carbon on a north-south transect in western
- Canada. European Journal of Soil Science, 53(3), 393–403. https://doi.org/10.1046/j.1365-2389.2002.00444.x

  Bodelier, P. L. E., & Laanbroek, H. J. (2004). Nitrogen as a regulatory factor of methane oxidation in soils and sediments. FEMS Microbiology Ecology, 47(3), 265–277. https://doi.org/10.1016/S0168-6496(03)00304-0
- Bogard, M. J., Kuhn, C. D., Johnston, S. E., Striegl, R. G., Holtgrieve, G. W., Dornblaser, M. M., et al. (2019). Negligible cycling of terrestrial carbon in many lakes of the arid circumpolar landscape. *Nature Geoscience*, 12(3), 180–185. https://doi.org/10.1038/s41561-019-0299-5
- Bridgham, S. D., Cadillo-Quiroz, H., Keller, J. K., & Zhuang, Q. (2013). Methane emissions from wetlands: Biogeochemical, microbial, and modeling perspectives from local to global scales. *Global Change Biology*, 19(5), 1325–1346. https://doi.org/10.1111/gcb.12131
- Bröder, L., Keskitalo, K., Zolkos, S., Shakil, S., Tank, S. E., Kokelj, S. V., et al. (2021). Preferential export of permafrost-derived organic matter as retrogressive thaw slumping intensifies. *Environmental Research Letters*, 32(5), 054059. https://doi.org/10.1088/1748-9326/abee4b
- Burn, C. R., & Kokelj, S. V. (2009). The environment and permafrost of the Mackenzie Delta area. *Permafrost and Periglacial Processes*, 20(2), 83–105. https://doi.org/10.1002/ppp.655
- Calmels, D., Gaillardet, J., Brenot, A., & France-Lanord, C. (2007). Sustained sulfide oxidation by physical erosion processes in the Mackenzie River basin: Climatic perspectives. *Geology*, 35(11), 1003–1006. https://doi.org/10.1130/G24132A.1
- Campeau, A., Bishop, K., Amvrosiadi, N., Billett, M. F., Garnett, M. H., Laudon, H., et al. (2019). Current forest carbon fixation fuels stream CO<sub>2</sub> emissions. *Nature Communications*, 10(1), 1876. https://doi.org/10.1038/s41467-019-09922-3
- Campeau, A., Bishop, K., Nilsson, M. B., Klemedtsson, L., Laudon, H., Leith, F. I., et al. (2018). Stable carbon isotopes reveal soil-stream DIC linkages in contrasting headwater catchments. *Journal of Geophysical Research: Biogeosciences*, 123(1), 149–167. https://doi.org/10.1002/2017JG004083
- Campeau, A., Lapierre, J.-F., Vachon, D., & del Giorgio, P. A. (2014). Regional contribution of CO<sub>2</sub> and CH<sub>4</sub> fluxes from the fluvial network in a lowland boreal landscape of Québec. *Global Biogeochemical Cycles*, 28(1), 57–69. https://doi.org/10.1002/2013GB004685
- Chapin, F. S., Woodwell, G. M., Randerson, J. T., Rastetter, E. B., Lovett, G. M., Baldocchi, D. D., et al. (2006). Reconciling carbon-cycle concepts, terminology, and methods. *Ecosystems*, 9(7), 1041–1050. https://doi.org/10.1007/s10021-005-0105-7
- Chin, K. S., Lento, J., Culp, J. M., Lacelle, D., & Kokelj, S. V. (2016). Permafrost thaw and intense thermokarst activity decreases abundance of stream benthic macroinvertebrates. *Global Change Biology*, 22(8), 2715–2728. https://doi.org/10.1111/gcb.13225
- Clark, P. U., Dyke, A. S., Shakun, J. D., Carlson, A. E., Clark, J., Wohlfarth, B., et al. (2009). The last glacial maximum. *Science*, 325(5941), 710–714. https://doi.org/10.1126/science.1172873
- Cole, J. J., & Caraco, N. F. (2001). Carbon in catchments: Connecting terrestrial carbon losses with aquatic metabolism. Marine and Freshwater Research, 52(1), 101–110. https://doi.org/10.1071/MF00084
- Connon, R. F., Chasmer, L., Haughton, E., Helbig, M., Hopkinson, C., Sonnentag, O., & Quinton, W. L. (2021). The implications of permafrost thaw and land cover change on snow water equivalent accumulation, melt and runoff in discontinuous permafrost peatlands. *Hydrological Processes*, 35(9), e14363. https://doi.org/10.1002/hyp.14363
- Côté, M. M., Duchesne, C., Wright, J. F., & Ednie, M. (2013). Digital compilation of the surficial sediments of the Mackenzie Valley corridor, Yukon Coastal Plain, and the Tuktoyaktuk Peninsula (No. 7289). https://doi.org/10.4095/292494
- Crawford, J. T., Loken, L. C., West, W. E., Crary, B., Spawn, S. A., Gubbins, N., et al. (2017). Spatial heterogeneity of within-stream methane concentrations. *Journal of Geophysical Research: Biogeosciences*, 122(5), 1036–1048. https://doi.org/10.1002/2016JG003698
- Crawford, J. T., Striegl, R. G., Wickland, K. P., Dornblaser, M. M., & Stanley, E. H. (2013). Emissions of carbon dioxide and methane from a headwater stream network of interior Alaska. *Journal of Geophysical Research: Biogeosciences*, 118(2), 482–494. https://doi.org/10.1002/jgrg.20034
- Crites, H., Kokelj, S. V., & Lacelle, D. (2020). Icings and groundwater conditions in permafrost catchments of northwestern Canada. Scientific Reports, 10(1), 3283. https://doi.org/10.1038/s41598-020-60322-w
- Drake, T. W., Guillemette, F., Hemingway, J. D., Chanton, J. P., Podgorski, D. C., Zimov, N. S., & Spencer, R. G. M. (2018). The ephemeral signature of permafrost carbon in an Arctic fluvial network. *Journal of Geophysical Research: Biogeosciences*, 123(5), 1–11. https://doi.org/10.1029/2017JG004311

ZOLKOS ET AL. 17 of 21

- Drake, T. W., Tank, S. E., Zhulidov, A. V., Holmes, R. M., Gurtovaya, T., & Spencer, R. G. M. (2018). Increasing alkalinity export from large Russian Arctic rivers. Environmental Science & Technology, 52(15), 8302–8308. https://doi.org/10.1021/acs.est.8b01051
- Duc, N. T., Silverstein, S., Lundmark, L., Reyier, H., Crill, P., & Bastviken, D. (2013). Automated flux chamber for investigating gas flux at water-air interfaces. *Environmental Science & Technology*, 47(2), 968–975. https://doi.org/10.1021/es303848x
- Duk-Rodkin, A., & Hughes, O. L. (1992a). Surficial geology, Arctic Red River, District of Mackenzie, Northwest Territories. Geological Survey of Canada
- Duk-Rodkin, A., & Hughes, O. L. (1992b). Surficial geology, Fort McPherson-Bell River, Yukon-Northwest Territories. Geological Survey of Canada.
- Ecosystem Classification Group. (2009). Ecological regions of the Northwest Territories: Taiga Plains (p. 173). Department of Environment and Natural Resources, Govt. of the Northwest Territories.
- Ecosystem Classification Group. (2010). Ecological regions of the Northwest Territories: Cordillera(p. 245). Department of Environment and Natural Resources, Govt. of the Northwest Territories.
- Ehlers, J., Gibbard, P. L., & Hughes, P. D. (2011). Quaternary glaciations Extent and chronology a closer look (Vol. 15). Elsevier. https://doi. org/10.1016/B978-0-444-53447-7.00001-5
- Goñi, M. A., Yunker, M. B., Macdonald, R. W., & Eglinton, T. I. (2005). The supply and preservation of ancient and modern components of organic carbon in the Canadian Beaufort Shelf of the Arctic Ocean. Marine Chemistry, 93(1), 53–73. https://doi.org/10.1016/j.marchem.2004.08.001
- Gordon, N. D., McMahon, T. A., Finlayson, B. L., Gippel, C. J., & Nathan, R. J. (2004). Stream hydrology: An introduction for ecologists (2nd ed.). Wiley.
- Hesslein, R. H., Rudd, J. W. M., Kelly, C., Ramlal, P., & Hallard, K. A. (1991). Carbon dioxide pressure in surface waters of Canadian lakes. In S. C. Wilhelms & J. S. Gulliver (Eds.), Air-water mass transfer: Selected papers from the second international symposium on gas transfer at water surfaces (pp. 413–431). American Society of Civil Engineers.
- Hicks Pries, C. E., Schuur, E. A. G., & Crummer, K. G. (2013). Thawing permafrost increases old soil and autotrophic respiration in tundra: Partitioning ecosystem respiration using  $\delta^{13}$ C and  $\Delta^{14}$ C. Global Change Biology, 19(2), 649–661. https://doi.org/10.1111/gcb.12058
- Hilton, R. G., Galy, V., Gaillardet, J., Dellinger, M., Bryant, C., O'Regan, M., et al. (2015). Erosion of organic carbon in the Arctic as a geological carbon dioxide sink. *Nature*, 524(7563), 84–87. https://doi.org/10.1038/nature14653
- Horan, K., Hilton, R. G., Dellinger, M., Tipper, E., Galy, V., Calmels, D., et al. (2019). Carbon dioxide emissions by rock organic carbon oxidation and the net geochemical carbon budget of the Mackenzie River Basin. *American Journal of Science*, 319(6), 473–499. https://doi.org/10.2475/06.2019.02
- Hugelius, G., Bockheim, J. G., Camill, P., Elberling, B., Grosse, G., Harden, J. W., et al. (2013). A new data set for estimating organic carbon storage to 3 m depth in soils of the northern circumpolar permafrost region. *Earth System Science Data*, 5(2), 393–402. https://doi.org/10.5194/
- Hugelius, G., Loisel, J., Chadburn, S., Jackson, R. B., Jones, M., MacDonald, G., et al. (2020). Large stocks of peatland carbon and nitrogen are vulnerable to permafrost thaw. *Proceedings of the National Academy of Sciences*, 117(34), 20438–20446. https://doi.org/10.1073/pnas.1916387117
- Hugelius, G., Strauss, J., Zubrzycki, S., Harden, J. W., Schuur, E. A. G., Ping, C.-L., et al. (2014). Estimated stocks of circumpolar permafrost carbon with quantified uncertainty ranges and identified data gaps. *Biogeosciences*, 11(23), 6573–6593. https://doi.org/10.5194/bg-11-6573-2014
- Humborg, C., Mörth, C.-M., Sundbom, M., Borg, H., Blenckner, T., Giesler, R., & Ittekkot, V. (2010). CO<sub>2</sub> supersaturation along the aquatic conduit in Swedish watersheds as constrained by terrestrial respiration, aquatic respiration and weathering. Global Change Biology, 16(7), 1966–1978. https://doi.org/10.1111/j.1365-2486.2009.02092.x
- Hutchins, R. H. S., Prairie, Y. T., & del Giorgio, P. A. (2021). The relative importance of seasonality versus regional and network-specific properties in determining the variability of fluvial CO<sub>2</sub>, CH<sub>4</sub> and dissolved organic carbon across boreal Québec. *Aquatic Sciences*, 83(4), 72. https://doi.org/10.1007/s00027-021-00830-7
- Hutchins, R. H. S., Tank, S. E., Olefeldt, D., Quinton, W. L., Spence, C., Dion, N., et al. (2020). Fluvial CO<sub>2</sub> and CH<sub>4</sub> patterns across wildfire-disturbed ecozones of subarctic Canada: Current status and implications for future change. *Global Change Biology*, 26(4), 2304–2319. https://doi.org/10.1111/gcb.14960
- Karlsson, J., Serikova, S., Vorobyev, S. N., Rocher-Ros, G., Denfeld, B., & Pokrovsky, O. S. (2021). Carbon emission from Western Siberian inland waters. *Nature Communications*, 12(1), 825. https://doi.org/10.1038/s41467-021-21054-1
- Keskitalo, K. H., Bröder, L., Jong, D., Zimov, N., Davydova, A., Davydov, S., et al. (2022). Seasonal variability in particulate organic carbon degradation in the Kolyma River, Siberia. Environmental Research Letters, 17(3), 034007. https://doi.org/10.1088/1748-9326/ac4f8d
- Keskitalo, K. H., Bröder, L., Shakil, S., Zolkos, S., Tank, S. E., van Dongen, B. E., et al. (2021). Downstream evolution of particulate organic matter composition from permafrost thaw slumps. Frontiers of Earth Science, 9, 642675. https://doi.org/10.3389/feart.2021.642675
- Kimball, J. S., Jones, L. A., Kundig, T., & Reichle, R. (2018). SMAP L4 global daily 9 km EASE-grid carbon net ecosystem exchange, version 4 [Data set]. NASA National Snow and Ice Data Center Distributed Active Archive Center. https://doi.org/10.5067/9831n0jgvaf6
- King, G. (1997). Responses of atmospheric methane consumption by soils to global climate change. *Global Change Biology*, 3(4), 351–362. https://doi.org/10.1046/j.1365-2486.1997.00090.x
- Kokelj, S. V., Kokoszka, J., van der Sluijs, J., Rudy, A. C. A., Tunnicliffe, J., Shakil, S., et al. (2021). Thaw-driven mass wasting couples slopes with downstream systems, and effects propagate through Arctic drainage networks. *The Cryosphere*, 15(7), 3059–3081. https://doi. org/10.5194/tc-15-3059-2021
- Kokelj, S. V., Lacelle, D., Lantz, T. C., Tunnicliffe, J., Malone, L., Clark, I. D., & Chin, K. S. (2013). Thawing of massive ground ice in mega slumps drives increases in stream sediment and solute flux across a range of watershed scales. *Journal of Geophysical Research: Earth Surface*, 118(2), 681–692. https://doi.org/10.1002/jgrf.20063
- Kokelj, S. V., Lantz, T. C., Tunnicliffe, J., Segal, R., & Lacelle, D. (2017). Climate-driven thaw of permafrost preserved glacial landscapes, northwestern Canada. Geology, 45(4), 371–374. https://doi.org/10.1130/G38626.1
- Kokelj, S. V., Tunnicliffe, J., Lacelle, D., Lantz, T. C., Chin, K. S., & Fraser, R. (2015). Increased precipitation drives mega slump development and destabilization of ice-rich permafrost terrain, northwestern Canada. Global and Planetary Change, 129, 56–68. https://doi.org/10.1016/j.gloplacha.2015.02.008
- Kokelj, S. V., Tunnicliffe, J. F., & Lacelle, D. (2017). The Peel Plateau of Northwestern Canada: An ice-rich hummocky moraine landscape in transition. In O. Slaymaker (Ed.), Landscapes and landforms of western Canada (pp. 109–122). Springer International Publishing. https://doi.org/10.1007/978-3-319-44595-3
- Kuhn, M. A., Varner, R. K., Bastviken, D., Crill, P., MacIntyre, S., Turetsky, M., et al. (2021). BAWLD-CH<sub>4</sub>: A comprehensive dataset of methane fluxes from boreal and Arctic ecosystems. Earth System Science Data Discussions. https://doi.org/10.5194/essd-2021-141

ZOLKOS ET AL. 18 of 21

- Lacelle, D., Lauriol, B., Zazula, G., Ghaleb, B., Utting, N., & Clark, I. D. (2013). Timing of advance and basal condition of the Laurentide Ice Sheet during the last glacial maximum in the Richardson Mountains, NWT. *Quaternary Research*, 80(2), 274–283. https://doi.org/10.1016/j. yqres.2013.06.001
- Lamhonwah, D., Lafrenière, M. J., Lamoureux, S. F., & Wolfe, B. B. (2017). Evaluating the hydrological and hydrochemical responses of a High Arctic catchment during an exceptionally warm summer. *Hydrological Processes*, 31(12), 2296–2313. https://doi.org/10.1002/hyp.11191
- Levenstein, B., Culp, J. M., & Lento, J. (2018). Sediment inputs from retrogressive thaw slumps drive algal biomass accumulation but not decomposition in Arctic streams, NWT. Freshwater Biology, 63(10), 1300–1315. https://doi.org/10.1111/fwb.13158
- Liebner, S., & Svenning, M. M. (2013). Environmental transcription of *mmoX* by methane-oxidizing *Proteobacteria* in a subarctic palsa peatland. *Applied and Environmental Microbiology*, 79(2), 701–706. https://doi.org/10.1128/AEM.02292-12
- Lipovsky, P. S., & Bond, J. D. (2014). Yukon digital surficial geology compilation, digital release 1. Yukon Geological Survey. Retrieved from http://data.geology.gov.yk.ca/Compilation/8
- Littlefair, C. A., Tank, S. E., & Kokelj, S. V. (2017). Retrogressive thaw slumps temper dissolved organic carbon delivery to streams of the Peel Plateau. NWT, Canada. *Biogeosciences*, 14(23), 5487–5505. https://doi.org/10.5194/bg-14-5487-2017
- Lundin, E. J., Klaminder, J., Giesler, R., Persson, A., Olefeldt, D., Heliasz, M., et al. (2016). Is the subarctic landscape still a carbon sink? Evidence from a detailed catchment balance. Geophysical Research Letters, 43(5), 1988–1995. https://doi.org/10.1002/2015GL066970
- Lurry, D. L., & Kolbe, C. M. (2000). Interagency field manual for the collection of water-quality data (No. OFR 00-213). USGS.
- Malone, L., Lacelle, D., Kokelj, S., & Clark, I. D. (2013). Impacts of hillslope thaw slumps on the geochemistry of permafrost catchments (Stony Creek watershed, NWT, Canada). Chemical Geology, 356, 38–49. https://doi.org/10.1016/j.chemgeo.2013.07.010
- McGuire, A. D., Genet, H., Lyu, Z., Pastick, N., Stackpoole, S., Birdsey, R., et al. (2018). Assessing historical and projected carbon balance of Alaska: A synthesis of results and policy/management implications. *Ecological Applications*, 28(6), 1396–1412. https://doi.org/10.1002/eap.1768
- Natali, S. M., Watts, J. D., Rogers, B. M., Potter, S., Ludwig, S. M., Selbmann, A.-K., et al. (2019). Large loss of CO<sub>2</sub> in winter observed across the northern permafrost region. *Nature Climate Change*, 9(11), 852–857. https://doi.org/10.1038/s41558-019-0592-8
- Norris, D. K. (1985). Geology of the Northern Yukon and Northwestern District of Mackenzie. Geological Survey of Canada.
- Oksanen, J., Blanchet, F. G., Friendly, M., Kindt, R., Legendre, P., McGlinn, D., et al. (2018). Package 'vegan' (Version 2.4-6). Retrieved from http://CRAN.R-project.org/package=vegan
- Olefeldt, D., Goswami, S., Grosse, G., Hayes, D., Hugelius, G., Kuhry, P., et al. (2016). Circumpolar distribution and carbon storage of thermokarst landscapes. *Nature Communications*, 7(1), 13043. https://doi.org/10.1038/ncomms13043
- Pallandt, M. M. T. A., Kumar, J., Mauritz, M., Schuur, E. A. G., Virkkala, A.-M., Celis, G., et al. (2022). Representativeness assessment of the pan-Arctic eddy covariance site network and optimized future enhancements. *Biogeosciences*, 19(3), 559–583. https://doi.org/10.5194/ber.10.559.2022
- Plaza, C., Pegoraro, E., Bracho, R., Celis, G., Crummer, K. G., Hutchings, J. A., et al. (2019). Direct observation of permafrost degradation and rapid soil carbon loss in tundra. *Nature Geoscience*, 12(8), 627–631. https://doi.org/10.1038/s41561-019-0387-6
- R Core Team. (2018). R: A language and environment for statistical computing. R Foundation for Statistical Computing. Retrieved from http://www.r-project.org/
- Rocher-Ros, G., Sponseller, R. A., Lidberg, W., Mörth, C., & Giesler, R. (2019). Landscape process domains drive patterns of CO<sub>2</sub> evasion from river networks. *Limnology and Oceanography Letters*, 4(4), 87–95. https://doi.org/10.1002/lo12.10108
- Running, S. W., Mu, Q., & Zhao, M. (2015). MOD17A2H MODIS/terra gross primary productivity 8-day L4 global 500 m SIN grid V006 [Data set]. https://doi.org/10.5067/MODIS/MOD17A2H.006
- Schädel, C., Bader, M. K.-F., Schuur, E. A. G., Biasi, C., Bracho, R., Čapek, P., et al. (2016). Potential carbon emissions dominated by carbon dioxide from thawed permafrost soils. *Nature Climate Change*, 6(10), 950–953. https://doi.org/10.1038/nclimate3054
- Segal, R. A., Lantz, T. C., & Kokelj, S. V. (2016). Acceleration of thaw slump activity in glaciated landscapes of the Western Canadian Arctic. Environmental Research Letters, 11(3), 034025. https://doi.org/10.1088/1748-9326/11/3/034025
- Shakil, S., Tank, S., Vonk, J., & Zolkos, S. (2021). Low biodegradability of particulate organic carbon mobilized from thaw slumps on the Peel Plateau, NT, and possible chemosynthesis and sorption effects. *Biogeosciences Discussions*. https://doi.org/10.5194/bg-2021-150
- Shakil, S., Tank, S. E., Kokelj, S. V., Vonk, J. E., & Zolkos, S. (2020). Particulate dominance of organic carbon mobilization from thaw slumps on the Peel Plateau, NT: Quantification and implications for stream systems and permafrost carbon release. *Environmental Research Letters*, 15(11), 114019. https://doi.org/10.1088/1748-9326/abac36
- Shakil, S., Tank, S. E., Vonk, J. E., & Zolkos, S. (2022). Low biodegradability of particulate organic carbon mobilized from thaw slumps on the Peel Plateau, NT, and possible chemosynthesis and sorption effects. *Biogeosciences*, 19(7), 1871–1890. https://doi.org/10.5194/ bg-19-1871-2022
- Shaver, G. R., Billings, W. D., Chapin, F. S., Giblin, A. E., Nadelhoffer, K. J., Oechel, W. C., & Rastetter, E. B. (1992). Global change and the carbon balance of Arctic ecosystems. BioScience, 42(6), 433–441. https://doi.org/10.2307/1311862
- Smith, C. A. S., Meikle, J. C., & Roots, C. F. (2004). Ecoregions of the Yukon Territory: Biophysical properties of Yukon landscapes. Agriculture and Agri-Food Canada.
- Song, C., & Wang, G. (2021). Land carbon sink of the Tibetan Plateau may be overestimated without accounting for the aquatic carbon export. Proceedings of the National Academy of Sciences, 118(46), e2114694118. https://doi.org/10.1073/pnas.2114694118
- Song, C., Wang, G., Hu, Z., Zhang, T., Huang, K., Chen, X., & Li, Y. (2020). Net ecosystem carbon budget of a grassland ecosystem in central Qinghai-Tibet Plateau: Integrating terrestrial and aquatic carbon fluxes at catchment scale. *Agricultural and Forest Meteorology*, 290, 108021. https://doi.org/10.1016/j.agrformet.2020.108021
- Stackpoole, S. M., Butman, D. E., Clow, D. W., Verdin, K. L., Gaglioti, B. V., Genet, H., & Striegl, R. G. (2017). Inland waters and their role in the carbon cycle of Alaska. *Ecological Applications*, 27(5), 1403–1420. https://doi.org/10.1002/eap.1552
- Strauss, J., Schirrmeister, L., Grosse, G., Fortier, D., Hugelius, G., Knoblauch, C., et al. (2017). Deep Yedoma permafrost: A synthesis of depositional characteristics and carbon vulnerability. *Earth-Science Reviews*, 172, 75–86. https://doi.org/10.1016/j.earscirev.2017.07.007
- Striegl, R. G., Aiken, G. R., Dornblaser, M. M., Raymond, P. A., & Wickland, K. P. (2005). A decrease in discharge-normalized DOC export by the Yukon River during summer through autumn. *Geophysical Research Letters*, 32(21), 1–4. https://doi.org/10.1029/2005GL024413
- Striegl, R. G., Dornblaser, M. M., Aiken, G. R., Wickland, K. P., & Raymond, P. A. (2007). Carbon export and cycling by the Yukon, Tanana, and Porcupine rivers, Alaska, 2001–2005. Water Resources Research, 43(2), 1–9. https://doi.org/10.1029/2006WR005201
- Striegl, R. G., Dornblaser, M. M., McDonald, C. P., Rover, J. R., & Stets, E. G. (2012). Carbon dioxide and methane emissions from the Yukon River system. Global Biogeochemical Cycles, 26(4), 1–11. https://doi.org/10.1029/2012GB004306

ZOLKOS ET AL. 19 of 21

- Tank, S. E., Raymond, P. A., Striegl, R. G., McClelland, J. W., Holmes, R. M., Fiske, G. J., & Peterson, B. J. (2012). A land-to-ocean perspective on the magnitude, source and implication of DIC flux from major Arctic rivers to the Arctic Ocean. *Global Biogeochemical Cycles*, 26(4), 1–15. https://doi.org/10.1029/2011GB004192
- Tank, S. E., Striegl, R. G., McClelland, J. W., & Kokelj, S. V. (2016). Multi-decadal increases in dissolved organic carbon and alkalinity flux from the Mackenzie drainage basin to the Arctic Ocean. *Environmental Research Letters*, 11(5), 054015. https://doi.org/10.1088/1748-9326/11/5/054015
- Tank, S. E., Vonk, J. E., Walvoord, M. A., McClelland, J. W., Laurion, I., & Abbott, B. W. (2020). Landscape matters: Predicting the biogeochemical effects of permafrost thaw on aquatic networks with a state factor approach. *Permafrost and Periglacial Processes*, 31(3), 358–370. https://doi.org/10.1002/ppp.2057
- Terhaar, J., Orr, J. C., Ethé, C., Regnier, P., & Bopp, L. (2019). Simulated Arctic Ocean response to doubling of riverine carbon and nutrient delivery. *Global Biogeochemical Cycles*, 33(8), 1048–1070. https://doi.org/10.1029/2019GB006200
- Toohey, R. C., Herman-Mercer, N. M., Schuster, P. F., Mutter, E. A., & Koch, J. C. (2016). Multidecadal increases in the Yukon River Basin of chemical fluxes as indicators of changing flowpaths, groundwater, and permafrost. *Geophysical Research Letters*, 43(23), 12120–12130. https://doi.org/10.1002/2016GL070817
- Turetsky, M. R., Abbott, B. W., Jones, M. C., Walter Anthony, K., Olefeldt, D., Schuur, E. A. G., et al. (2020). Carbon release through abrupt permafrost thaw. *Nature Geoscience*, 13(2), 138–143. https://doi.org/10.1038/s41561-019-0526-0
- van der Sluijs, J., Kokelj, S. V., Fraser, R. H., Tunnicliffe, J., & Lacelle, D. (2018). Permafrost terrain dynamics and infrastructure impacts revealed by UAV photogrammetry and thermal imaging. *Remote Sensing*, 10(1734), 1–30. https://doi.org/10.3390/rs10111734
- Virkkala, A., Aalto, J., Rogers, B. M., Tagesson, T., Treat, C. C., Natali, S. M., et al. (2021). Statistical upscaling of ecosystem CO<sub>2</sub> fluxes across the terrestrial tundra and boreal domain: Regional patterns and uncertainties. Global Change Biology, 27(17), 4040–4059. https://doi.org/10.1111/gcb.15659
- Voigt, C., Lamprecht, R. E., Marushchak, M. E., Lind, S. E., Novakovskiy, A., Aurela, M., et al. (2017). Warming of subarctic tundra increases emissions of all three important greenhouse gases Carbon dioxide, methane, and nitrous oxide. Global Change Biology, 23(8), 3121–3138. https://doi.org/10.1111/gcb.13563
- Vonk, J. E., Tank, S. E., & Walvoord, M. A. (2019). Integrating hydrology and biogeochemistry across frozen landscapes. *Nature Communications*, 10(1), 5377. https://doi.org/10.1038/s41467-019-13361-5
- Wallin, M. B., Grabs, T., Buffam, I., Laudon, H., Ågren, A., Öquist, M. G., & Bishop, K. (2013). Evasion of CO<sub>2</sub> from streams The dominant component of the carbon export through the aquatic conduit in a boreal landscape. *Global Change Biology*, 19(3), 785–797. https://doi.org/10.1111/gcb.12083
- Walter Anthony, K., Daanen, R., Anthony, P., Schneider von Deimling, T., Ping, C.-L., Chanton, J. P., & Grosse, G. (2016). Methane emissions proportional to permafrost carbon thawed in Arctic lakes since the 1950s. *Nature Geoscience*, 9(9), 679–682. https://doi.org/10.1038/ngeo2795
- Watts, J., Natali, S. M., Minions, C., Risk, D., Arndt, K. A., Zona, D., et al. (2021). Soil respiration strongly offsets carbon uptake in Alaska and Northwest Canada. *Environmental Research Letters*, 16(8), 084051. https://doi.org/10.1088/1748-9326/ac1222
- Wild, B., Schnecker, J., Alves, R. J. E., Barsukov, P., Bárta, J., Čapek, P., et al. (2014). Input of easily available organic C and N stimulates microbial decomposition of soil organic matter in arctic permafrost soil. Soil Biology and Biochemistry, 75, 143–151. https://doi.org/10.1016/j. soilbio.2014.04.014
- Zolkos, S., Tank, S., Kokelj, S. V., Striegl, R., Shakil, S., Voigt, C., et al. (2022). Stream and river summertime water quality, carbon, nutrients, isotopes, gases, and constituent export in 33 permafrost-affected watersheds across 4 ecoregions in the western Canadian Arctic (June–August, 2015). Polar Data Catalogue. https://doi.org/10.21963/13279
- Zolkos, S., & Tank, S. E. (2020). Experimental evidence that permafrost thaw history and mineral composition shape abiotic carbon cycling in thermokarst-affected stream networks. Frontiers of Earth Science, 8(152), 1–17. https://doi.org/10.3389/feart.2020.00152
- Zolkos, S., Tank, S. E., & Kokelj, S. V. (2018). Mineral weathering and the permafrost carbon-climate feedback. Geophysical Research Letters, 45(18), 9623–9632. https://doi.org/10.1029/2018GL078748
- Zolkos, S., Tank, S. E., Striegl, R. G., & Kokelj, S. V. (2019). Thermokarst effects on carbon dioxide and methane fluxes in streams on the Peel Plateau (NWT, Canada). *Journal of Geophysical Research: Biogeosciences*, 124(7), 2019JG005038. https://doi.org/10.1029/2019JG005038
- Zolkos, S., Tank, S. E., Striegl, R. G., Kokelj, S. V., Kokoszka, J., Estop-Aragonés, C., & Olefeldt, D. (2020). Thermokarst amplifies fluvial inorganic carbon cycling and export across watershed scales on the Peel Plateau, Canada. *Biogeosciences*, 17(20), 5163–5182. https://doi. org/10.5194/bg-2020-111

## **References From the Supporting Information**

- EPA. (2000). Guidance for data quality Assessment (No. EPA QA/G-9 QA00 Version). Environmental Protection Agency.
- Gorelick, N., Hancher, M., Dixon, M., Ilyushchenko, S., Thau, D., & Moore, R. (2017). Google Earth Engine: Planetary-scale geospatial analysis for everyone. *Remote Sensing of Environment*, 202, 18–27. https://doi.org/10.1016/j.rse.2017.06.031
- Gray, J. R., & Landers, M. N. (2014). Measuring suspended sediment. In Comprehensive water quality and purification (pp. 157–204). Elsevier. https://doi.org/10.1016/B978-0-12-382182-9.00012-8
- Helms, J. R., Stubbins, A., Ritchie, J. D., Minor, E. C., Kieber, D. J., & Mopper, K. (2008). Absorption spectral slopes and slope ratios as indicators of molecular weight, source, and photobleaching of chromophoric dissolved organic matter. *Limnology & Oceanography*, 53(3), 955–969. https://doi.org/10.4319/lo.2008.53.3.0955
- Hutchins, R. H. S., Prairie, Y. T., & del Giorgio, P. A. (2019). Large-scale landscape drivers of CO<sub>2</sub>, CH<sub>4</sub>, DOC, and DIC in boreal river networks. Global Biogeochemical Cycles, 33(2), 125–142. https://doi.org/10.1029/2018GB006106
- Ikawa, H., Nakai, T., Busey, R. C., Kim, Y., Kobayashi, H., Nagai, S., et al. (2015). Understory CO2, sensible heat, and latent heat fluxes in a black spruce forest in interior Alaska. *Agricultural and Forest Meteorology*, 214–215, 80–90. https://doi.org/10.1016/j.agrformet.2015.08.247
- Jin, L., Ogrinc, N., Hamilton, S. K., Szramek, K., Kanduc, T., & Walter, L. M. (2009). Inorganic carbon isotope systematics in soil profiles undergoing silicate and carbonate weathering (Southern Michigan, USA). Chemical Geology, 264(1-4), 139-153. https://doi.org/10.1016/j. chemgeo.2009.03.002
- Kobayashi, H., Ikawa, H., & Suzuki, R. (2016). AmeriFlux AmeriFlux US-Prr Poker Flat Research Range black spruce forest. https://doi.org/10.17190/AMF/1246153
- Lehn, G. O., Jacobson, A. D., Douglas, T. A., McClelland, J. W., Barker, A. J., & Khosh, M. S. (2017). Constraining seasonal active layer dynamics and chemical weathering reactions occurring in North Slope Alaskan watersheds with major ion and isotope (δ<sup>34</sup>S<sub>S04</sub>, δ<sup>13</sup>C<sub>DIC</sub>, <sup>87</sup>Sr/<sup>86</sup>Sr, δ<sup>44</sup>/<sup>40</sup>Ca, and δ<sup>44</sup>/<sup>42</sup>Ca) measurements. *Geochimica et Cosmochimica Acta*, 217, 399–420. https://doi.org/10.1016/j.gca.2017.07.042

ZOLKOS ET AL. 20 of 21

- Littlefair, C. A., & Tank, S. E. (2018). Biodegradability of thermokarst carbon in a till-associated, glacial margin landscape: The case of the Peel Plateau, NWT, Canada. *Journal of Geophysical Research: Biogeosciences, 123*(10), 3293–3307. https://doi.org/10.1029/2018JG004461
- Lorrain, A., Savoye, N., Chauvaud, L., Paulet, Y.-M., & Naulet, N. (2003). Decarbonation and preservation method for the analysis of organic C and N contents and stable isotope ratios of low-carbonated suspended particulate material. *Analytica Chimica Acta*, 491(2), 125–133. https://doi.org/10.1016/S0003-2670(03)00815-8
- Millero, F. J. (1979). The thermodynamics of the carbonate system in seawater. Geochimica et Cosmochimica Acta, 43(10), 1651–1661. https://doi.org/10.1016/0016-7037(79)90184-4
- Millero, F. J. (2010). Carbonate constants for estuarine waters. Marine and Freshwater Research, 61(2), 139. https://doi.org/10.1071/MF09254 Pierrot, D., Lewis, E., & Wallace, D. W. R. (2006). MS excel program developed for CO<sub>2</sub> system calculations. Carbon Dioxide Information
- Analysis Center, Oak Ridge National Laboratory, US Department of Energy, https://doi.org/10.3334/CDIAC/otg.CO2SYS\_XLS\_CDIAC105a
  Piper, A. M. (1944). A graphic procedure in the geochemical interpretation of water-analyses. Transactions American Geophysical Union.
- Piper, A. M. (1944). A graphic procedure in the geochemical interpretation of water-analyses. *Transactions American Geophysical Unio* 25(6), 914. https://doi.org/10.1029/TR025i006p00914
- Poulin, B. A., Ryan, J. N., & Aiken, G. R. (2014). Effects of iron on optical properties of dissolved organic matter. Environmental Science & Technology, 48(17), 10098–10106. https://doi.org/10.1021/es502670r
- Sander, R. (2015). Compilation of Henry's law constants (version 4.0) for water as solvent. Atmospheric Chemistry and Physics, 15(8), 4399–4981. https://doi.org/10.5194/acp-15-4399-2015
- Shakil, S., Tank, S., Kokelj, S., & Zolkos, S. (2020). The effect of retrogressive thaw slumps on the delivery of organic matter and nutrients to downstream freshwater systems in the Peel Plateau region, Northwest Territories [Data set]. Canadian Cryospheric Information Network. https://doi.org/10.21963/13160
- Stainton, M. P. (1973). A syringe gas-stripping procedure for gas-chromatographic determination of dissolved inorganic and organic carbon in Fresh water and carbonates in sediments. *Journal of the Fisheries Research Board of Canada*, 30(10), 1441–1445. https://doi.org/10.1139/f73.234
- Striegl, R. G., Kortelainen, P., Chanton, J. P., Wickland, K. P., Bugna, G. C., & Rantakari, M. (2001). Carbon dioxide partial pressure and <sup>13</sup>C content of north temperate and boreal lakes at spring ice melt. *Limnology & Oceanography*, 46(4), 941–945. https://doi.org/10.4319/
- Stubbins, A., Silva, L. M., Dittmar, T., & Van Stan, J. T. (2017). Molecular and optical properties of tree-derived dissolved organic matter in throughfall and stemflow from live oaks and eastern red cedar. Frontiers of Earth Science, 5(22), 1–13, https://doi.org/10.3389/feart.2017.00022
- Tank, S. E., Lesack, L. F. W., & Hesslein, R. H. (2009). Northern delta lakes as summertime CO<sub>2</sub> absorbers within the Arctic landscape. *Ecosystems*, 12(1), 144–157. https://doi.org/10.1007/s10021-008-9213-5
- Tondu, J. M. E., Turner, K. W., Wolfe, B. B., Hall, R. I., Edwards, T. W. D., & McDonald, I. (2013). Using water isotope tracers to develop the hydrological component of a long-term aquatic ecosystem monitoring program for a northern lake-rich landscape. Arctic Antarctic and Alpine Research, 45(4), 594–614. https://doi.org/10.1657/1938-4246-45.4.594
- Turner, K. W., Edwards, T. W. D., & Wolfe, B. B. (2014). Characterising runoff generation processes in a lake-rich thermokarst landscape (Old Crow Flats, Yukon, Canada) using δ<sup>18</sup>O, δ<sup>2</sup>H and d-excess measurements. *Permafrost and Periglacial Processes*, 25(1), 53–59. https://doi.org/10.1002/ppp.1802
- Vonk, J. E., Tank, S. E., Mann, P. J., Spencer, R. G. M., Treat, C. C., Striegl, R. G., et al. (2015). Biodegradability of dissolved organic carbon in permafrost soils and aquatic systems: A meta-analysis. *Biogeosciences*, 12(23), 6915–6930. https://doi.org/10.5194/bg-12-6915-2015
- Ward, C. P., & Cory, R. M. (2016). Complete and partial photo-oxidation of dissolved organic matter draining permafrost soils. *Environmental Science & Technology*, 50(7), 3545–3553. https://doi.org/10.1021/acs.est.5b05354
- Weishaar, J. L., Aiken, G. R., Bergamaschi, B. A., Fram, M. S., Fujii, R., & Mopper, K. (2003). Evaluation of specific ultraviolet absorbance as an indicator of the chemical composition and reactivity of dissolved organic carbon. *Environmental Science & Technology*, 37(20), 4702–4708. https://doi.org/10.1021/es030360x
- Weiss, R. F. (1974). Carbon dioxide in water and seawater: The solubility of a non-ideal gas. Marine Chemistry, 2(3), 203–215. https://doi.org/10.1016/0304-4203(74)90015-2
- Whiteside, J. H., Olsen, P. E., Eglinton, T. I., Cornet, B., McDonald, N. G., & Huber, P. (2011). Pangean great lake paleoecology on the cusp of the end-Triassic extinction. *Palaeogeography, Palaeoclimatology, Palaeoecology*, 301(1–4), 1–17. https://doi.org/10.1016/j.palaeo.2010.11.025
- Wickland, K. P., Aiken, G. R., Butler, K., Dornblaser, M. M., Spencer, R. G. M., & Striegl, R. G. (2012). Biodegradability of dissolved organic carbon in the Yukon River and its tributaries: Seasonality and importance of inorganic nitrogen. *Global Biogeochemical Cycles*, 26(4), 1–14. https://doi.org/10.1029/2012GB004342
- Wiesenburg, D. A., & Guinasso, N. L. (1979). Equilibrium solubilities of methane, carbon monoxide, and hydrogen in water and sea water. *Journal of Chemical and Engineering Data*, 24(4), 356–360. https://doi.org/10.1021/je60083a006
- Zuur, A. F. (2009). Mixed effects models and extensions in ecology with R. Springer.

ZOLKOS ET AL. 21 of 21